JOURNAL OF PETROLOGY | VOLUME 45 | NUMBER 7 | PAGES 1311–1338 | 2004 | DOI: 10.1093/petrology/egh020

The Problem of Dating High-pressure Metamorphism: a U–Pb Isotope and Geochemical Study on Eclogites and Related Rocks of the Mariánské Lázně Complex, Czech Republic

H. TIMMERMANN[1,2]*, V. ŠTĚDRÁ[3], A. GERDES[1], S. R. NOBLE[1], R. R. PARRISH[1,4] AND W. DÖRR[2]

[1]NERC ISOTOPE GEOSCIENCES LABORATORY, KEYWORTH, NOTTINGHAM NG12 5GG, UK

[2]IGL, JUSTUS LIEBIG UNIVERSITÄT, SENCKENBERGSTR. 3, D-35390 GIESSEN, GERMANY

[3]CZECH GEOLOGICAL SURVEY, PRAGUE, CZECH REPUBLIC

[4]DEPARTMENT OF GEOLOGY, UNIVERSITY OF LEICESTER, UNIVERSITY ROAD, LEICESTER LE1 7RH, UK

RECEIVED AUGUST 1, 2002; ACCEPTED JANUARY 21, 2004

This study presents new geochemical (major and trace element, Nd–Sr isotope) and U–Pb zircon, monazite, titanite and rutile data for various rock types (eclogite, high-pressure granulite, amphibolite, orthogneiss, leucosome) of the high-grade metamorphic Mariánské Lázně Complex in the western Bohemian Massif. Concordant U–Pb zircon analyses from the mafic to intermediate samples disclose the Mariánské Lázně Complex as a mixture of c. *540 Ma oceanic rocks juxtaposed at depth with lower-crustal rocks of the structurally overlying Teplá–Barrandian Unit. This interpretation refutes earlier models in which the Mariánské Lázně Complex was interpreted as a dismembered Cambro-Ordovician ophiolite complex affected by Variscan subduction. Metamorphic zircon in mafic rocks of the Mariánské Lázně Complex, as well as monazite from orthogneiss, and titanite in leucosome yield ages around 380 Ma. On the basis of detailed petrography and cathodoluminescence imaging we conclude that the* c. *380 Ma age reflects the timing of Variscan exhumation and associated decompression melting under upper amphibolite-facies to granulite-facies conditions. Thereby, the data derived from metamorphic zircon of eclogites and high-pressure granulite, unexpectedly, do not date the timing of eclogitization, which could have happened just before Variscan exhumation, or even shortly after Late Cadomian protolith formation.*

KEY WORDS: *Bohemian Massif; eclogites; geochemistry; U–Pb geochronology; zircon*

INTRODUCTION

Metamorphic rocks that formed at very high pressures, such as eclogites and high-pressure granulites, are the most important witnesses of the tectonothermal processes that happen within the generally inaccessible lower crust and lithospheric mantle. Studies of these kinds of high-pressure rocks, however, are hampered by the difficulty of precisely determining the age of the high-pressure event, and thus constraining the geodynamic evolution and tectonic setting in which these rocks formed. Eclogite-facies mineral assemblages form in rocks of all lithologies under the P–T conditions of the upper mantle (e.g. Eskola, 1920, 1939; Carswell, 1990), although the term eclogite is generally used for subducted mafic ocean crust, in which plagioclase decomposes to omphacitic clinopyroxene and garnet (Carswell, 1990). High-pressure granulites, in comparison, are generally viewed as rocks that have formed under conditions that are transitional between granulite and eclogite facies (e.g. Green & Ringwood, 1967; Ringwood, 1975); however, they occupy a different P–T field compared with eclogites, because they have formed under conditions with a higher thermal gradient (e.g. O'Brien & Rötzler, 2003, and references therein).

Because of the scarcity or absence of U-rich accessory minerals in mafic and ultramafic rocks, mafic eclogites,

*Corresponding author. Telephone: +49 (0641) 9936016. Fax: +49 (0641) 9936019. E-mail: Hilke.Timmermann@geolo.uni-giessen.de

generally the best preserved type of high-pressure rock, are commonly dated with the widely available Sm–Nd method. High $^{147}Sm/^{144}Nd$ ratios in garnets and clinopyroxene provide sufficient spread to allow calculation of Sm–Nd isochrons (e.g. Brueckner *et al.*, 1991; Burton & O'Nions, 1991; de Sigoyer *et al.*, 2000). To determine the timing of the high-pressure event, only those garnets or clinopyroxenes (or those zones within these minerals) that equilibrated during the high-pressure phase can be used. Although the eclogitization phase has been successfully determined by this method in several cases (e.g. Gebauer, 1990), Sm–Nd isochrons often reflect only cooling ages (e.g. Mezger *et al.*, 1992; Burton *et al.*, 1995). Closure temperatures for the Sm–Nd chronometer range from 600 to 700°C (e.g. Mezger *et al.*, 1992; Burton *et al.*, 1995). These temperatures are often reached in the course of exhumation, or during subsequent regional metamorphic events. However, instead of resetting by volume diffusion, the cooling ages are produced by isotopic equilibration during deformation-enhanced fluid circulation in the course of retrograde amphibolite-facies metamorphism (e.g. Ganguly *et al.*, 1998; Luais *et al.*, 2001). Another problem with the Sm–Nd chronometer is the possibility of isotopic disequilibrium in the Sm–Nd system in garnets, which can lead to ambiguous ages. This may arise because of (1) inclusions rich in rare earth elements (REE) or real variation in lattice concentrations (e.g. De Wolf *et al.*, 1996; Prince *et al.*, 2000; Luais *et al.*, 2001; Anczkiewicz *et al.*, 2002), or (2) strong heavy REE (HREE) zoning in garnet where Sm is partitioned only into the late phases of garnet growth (e.g. Lapen *et al.*, 2002; Schmitz *et al.*, 2002).

By comparison, U–Pb geochronology, especially of zircon, is the most widely used and most precise method of dating geological events, although this method can be difficult to apply to high-pressure rocks. Mafic rocks, such as those in oceanic crust, do not generally form zircon during protolith crystallization owing to the relatively low SiO_2 contents and the high solubility of Zr in mafic melts. Zr is incorporated into clinopyroxene and other igneous minerals (e.g. baddeleyite), and released only during metamorphic recrystallization or anatexis, at which time Zr and available SiO_2 commonly form metamorphic zircon (e.g. Davidson & van Breemen, 1988; Heaman & Parrish, 1991). Recent studies have discussed the possibility that in certain regions zircon may not grow during the high-pressure event but instead on the retrograde path, such as during exhumation in the presence of a melt (e.g. Roberts & Finger, 1997; Fernandez-Suarez *et al.*, 2002; Whitehouse & Platt, 2003). This uncertainty hinders the interpretation of the timing of collisional events and reconstruction of palaeogeography, especially in areas as tectonically complex as Variscan Central Europe (e.g. Franke *et al.*, 2000; and references therein). In the Bohemian Massif, for example, numerous eclogites are interpreted to have formed by subduction during Variscan ocean-floor closure; however, geochronological evidence for this hypothesis is scarce (e.g. O'Brien *et al.*, 1990). The Mariánské Lázně Complex (MLC) in the northwestern Bohemian Massif (Fig. 1), well known as the largest outcrop of mafic rocks in Variscan Central Europe, contains lenses of eclogitic rocks in an amphibolitic host that is exotic with respect to the surrounding continental rocks of the Saxothuringian Zone and the Teplá–Barrandian Unit (TBU; e.g. Jelínek *et al.*, 1997; Štědrá, 2001). Although few age data exist, the MLC is generally accepted to represent Early Ordovician ocean floor (e.g. Bowes & Aftalion, 1991) that experienced a complex Variscan tectonometamorphic evolution culminating in eclogite formation around 370 Ma (e.g. Beard *et al.*, 1995). By using U–Pb geochronology on eclogites and related rocks in the MLC, we will demonstrate not only the difficulty of dating high-pressure rocks in general, but also show that the MLC does not represent, as previously thought, an allochthon of Palaeozoic origin. Instead, the MLC was part of a Cadomian active margin of Gondwana that also included the TBU structurally above the MLC.

GEOLOGICAL SETTING

The high-grade metamorphic MLC lies at the northwestern edge of the Bohemian Massif (Fig. 1), located at the boundary between the 'continental' lower-grade Saxothuringian Zone in the NW and the medium-grade TBU in the SE (e.g. Jelínek *et al.*, 1997), with tectonic contacts to the Moldanubian Zone in the SW (e.g. Matte *et al.*, 1990). The MLC comprises different thrust-bound rock units with varying metamorphic grades that generally dip to the SE (e.g. Cháb, 1973; Kastl & Tonika, 1984). These include serpentinized peridotites, lower-grade amphibolites, higher-grade amphibolites with eclogite lenses, rare high-pressure granulites, amphibolitic schists with coronitic metagabbros, and intercalations of paragneisses and felsic orthogneisses (e.g. Fiala, 1958; Jelínek *et al.*, 1997; Štědrá, 2001).

Whereas the eclogite boudins and lenses occur mainly within the central MLC, more variable types of high-pressure rocks occur in the northern MLC in the area east of the Teplá Valley and north of the Otrocín Valley (Štědrá, 2001). The eclogite-facies mineral assemblage is garnet and relict omphacite, with kyanite, quartz, zoisite, and rutile as common constituents. Most eclogites have been overprinted by high-pressure granulite-facies metamorphism, followed by penetrative amphibolite-facies metamorphism during exhumation. On the basis of geochemical evidence, the eclogite protoliths were classified as mid-ocean ridge basalts (MORB) ranging from light REE (LREE)-depleted (N-MORB) to LREE-enriched

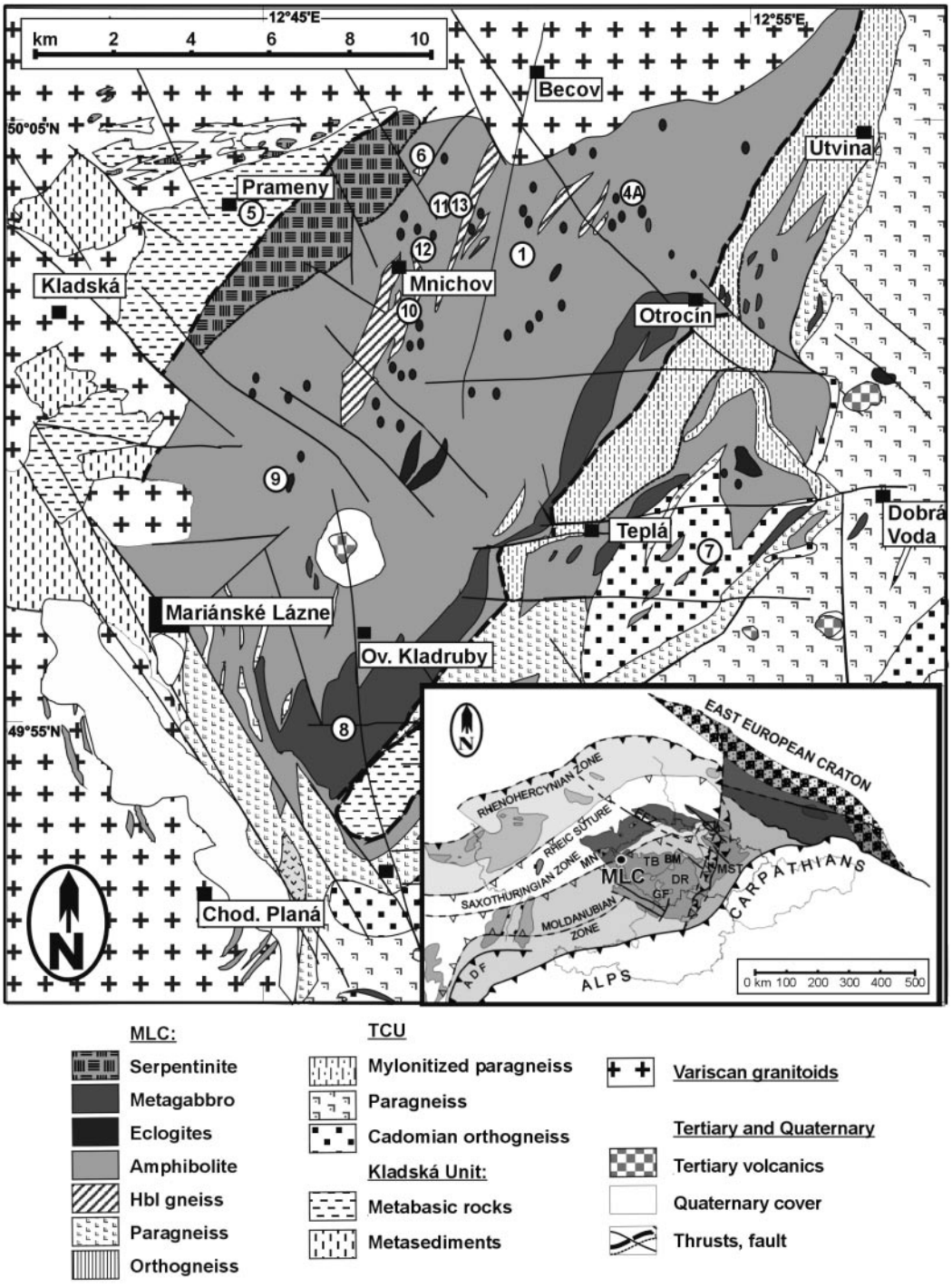

Fig. 1. Schematic geological map (Cháb *et al.*, 1997) of the Mariánské Lázně Complex (MLC) after Štědrá (2001). The inset is a geological map of the Czech Republic (scale 1:50 000; Tonika, 1998) showing the location of the MLC with respect to the Bohemian Massif (BM) and the main Variscan units of Central Europe (after Pharaoh, 1999). TB, Teplá–Barrandian; DR, Drosendorf unit; GF, Gföhl unit; MN, Münchberg Nappe; MST, Upper Silesian Massif; ADF, Alpine Deformation Front; EFZ, Elbe Fault Zone; TCU, Teplá Crystalline Unit.

(E-MORB) types (Kastl & Tonika, 1984; Beard *et al.*, 1995). The eclogites, however, make up only a small proportion compared with their hosts, the intermediate to mafic amphibolites. The amphibolites consist of several rock types grading into each other, and are generally interpreted to represent the thoroughly retrogressed equivalents of the associated eclogites and metagabbros (e.g. Kastl & Tonika, 1984; Jelínek *et al.*, 1997; Štědrá,

2001). Leucocratic orthogneisses are locally associated with the amphibolites. Although inclusions of amphibolite were observed within the orthogneisses, the contact relationships with the host rocks of the MLC are not clear (e.g. Kastl & Tonika, 1984; Jelínek *et al.*, 1997). In comparison with the eclogites, the orthogneisses studied do not exhibit any high-pressure mineral assemblages.

Constrictional fabrics within eclogitic lenses are interpreted as relict fabrics derived from slab pull during subduction (Zulauf, 1997*a*). The peak *P–T* conditions, during which the high-pressure assemblage Grt–Omp–Zo–Rt ± Ky ± Qtz formed, reached at least 16–18 kbar and 640–715°C (Jelínek *et al.*, 1997, and references therein; O'Brien, 1997). Complex textures in some of the eclogites indicate a high-pressure granulite-facies overprint, followed by medium-pressure granulite-facies, and finally by a penetrative amphibolite-facies metamorphism (e.g. O'Brien *et al.*, 1997). *P–T* conditions for these events were determined from retrograde assemblages and amphibolites to be in the range of 9–12 kbar and 600–780°C (Jelínek *et al.*, 1997, and references therein). The *P–T* path synthesized by Zulauf (1997*b*), using all of the available *P–T* data for this area, shows an isothermal decompression path with the temperature peak occurring after the pressure peak during medium-pressure granulite-facies metamorphism. However, the detailed petrological study of Štědrá (2001) indicates that eclogites, high-pressure granulites, metagabbros, and present-day amphibolite-facies rocks have contrasting *P–T* paths.

Only few geochronological data are available from the MLC. Although Fiala (1958) and Kastl & Tonika (1984) compared the rocks of the MLC with Proterozoic rocks of the Central Bohemian Massif, a U–Pb zircon age of 496 ± 1 Ma for a gabbro pegmatite (Bowes & Aftalion, 1991) has generally been taken as evidence for crystallization of the gabbros and other mafic host rocks of the MLC during early Ordovician rifting and associated ocean-floor formation, which formed the Amorican terrane assemblage (e.g. Jelínek *et al.*, 1997). Until the present study, late Proterozoic protolith ages have only been indicated by U–Pb multigrain zircon analyses from feldspathic gneisses in the MLC that yield an upper intercept age of 854 Ma but with a high error of 130 Ma as a result of mixed inheritance (Bowes & Aftalion, 1991). Beard *et al.* (1995) proposed the timing of eclogite formation (subduction during closure of the MLC ocean basin and collision of the Saxothuringian and Teplá–Barrandian plates) to be represented by Sm–Nd isochrons giving 367 ± 4 Ma for garnet and omphacite rim compositions and 377 ± 7 Ma for garnet and omphacite within eclogite. Based on petrographic evidence and mineral chemistry, older Sm–Nd ages from the mineral cores (409 ± 8 Ma, 420 ± 9 Ma) were interpreted to reflect either the timing of prograde metamorphism or a cryptic amphibolite-facies metamorphism during late Silurian convergence (Beard *et al.*, 1995). The younger, supposedly eclogite-facies, Sm–Nd ages agree within error with a U–Pb zircon lower intercept age of 362 +12/–9 Ma for Late Devonian–Early Carboniferous tectonothermal activity (Bowes & Aftalion, 1991). However, K–Ar and $^{40}Ar/^{39}Ar$ hornblende data, reflecting regional cooling below *c.* 500°C, give an age range from 380 to 370 Ma for the central MLC (Kreuzer *et al.*, 1992; Dallmeyer & Urban, 1994; Zulauf, 1997*b*; Bowes *et al.*, 2002). In the southeastern part of the MLC the K–Ar hornblende cooling ages are as old as 397 ± 5 Ma (Zulauf, 1997*b*). The cooling ages are thus similar to or even older than the Sm–Nd ages proposed to reflect eclogite-facies metamorphism.

SAMPLE DESCRIPTION

Localities (Fig. 1), mineral assemblages and *P–T* data of analysed samples are listed in Table 1.

Sample HT-99-4a is a fine- to medium-grained, high-pressure granulite of intermediate composition. The sample has a 'spotty' appearance as a result of a regular distribution of light-coloured, ellipsoidal, Al-rich domains in a darker matrix (Fig. 2a and b). The matrix (Fig. 2b) is composed of disseminated garnet, Na-rich clinopyroxene, plagioclase, quartz, secondary amphibole, kyanite, rutile and zoisite. Omphacite (Cpx I) is replaced by coarse-grained Cpx (II)–Pl symplectite and bleb-like intergrowth of plagioclase and Na-rich clinopyroxene. Garnet compositions vary slightly between the domains (lower pyrope component in matrix) as a result of different bulk compositions. Garnet is zoned in lighter domains (Fig. 2c) and homogeneous in the matrix.

Medium-grained, mafic eclogite HT-99-9 originates from the core of a large eclogite boudin surrounded by garnet-bearing gneisses that are intermediate in composition. Large garnet crystals are surrounded by narrow kelyphitic rims of green amphibole and Ca-rich plagioclase. Inclusion-rich cores and inclusion-free rims of the garnets, as well as weak compositional zoning, reflect a poly-stage growth and re-equilibration evolution (Fig. 3a). Early omphacitic clinopyroxene is replaced by partially amphibolitized plagioclase symplectites. At the contact between the matrix and quartz veins, symplectitic biotite, anorthite, and sillimanite replace a high-pressure mineral relict (probably phengite). Relict kyanite is surrounded by symplectitic spinel–anorthite or sillimanite/sapphirine–anorthite aggregates (Fig. 3b).

Garnet (diameter 0·5–2 mm) in sample HT-99-11, part of a well-preserved mafic eclogite boudin, forms up to 25% of the matrix. Large, zoned (Fig. 4a) garnet crystals have dark pink inclusion-rich cores and clear pale margins, reflecting a two-stage growth history. Small garnet

Table 1: Characteristics of samples analysed in this study, Mariánské Lázně Complex (MLC), Czech Republic

Sample no.	Locality	Rock type	Mineral assemblage [abbreviations after Kretz (1983)]	Thermobarometry	U–Pb geochronology (this study)/ interpretation
HT-99-1	roadcut W of Tisova	felsic Pl–Qtz–Ky leucosome in neck of retrogressed mafic eclogite boudin, L-fabric with NW/NNW lineation	Pl–Qtz–Grt–Ky–Ms–Hbl–Ttn–Zrn	6–10 kbar/560–620°C[6] (retrogression in eclogite)	378 ± 4 Ma (Ttn)/cryst. 366 ± 13 Ma (Ttn)/cooling
HT-99-4a	W of Mechov, north Otrocinsky Potok Creek	high-pressure (HP) granulite	Ab–Qtz–Grt–Omp–Ed–Hbl–Ky–Zo–Rt–Ilm–Spl–An–Ap–Zrn	HP: GrtI core, Pl, Omp 14–16 kbar/650–750°C[1,2] post-HP:GrtII rim-CpxII,Pl–Hbl 12–14 kbar/780–850°C[1,2]	546 ± 3 Ma (Zrn)/igneous 534 ± 2 Ma (Zrn)
HT-99-6	300 m N of road between Prameny and Louka, Pramensky Potok Creek	felsic orthogneiss overlying serpentinite body; MP metamorphism (no HP assemblages), distinct L-fabric	Pl–Kfs–Qtz–Bt–Ms–Chl–Grt–Zrn–Mnz	8–13 kbar[4]/640–740°C[3] 10–12 kbar[4]/550–680°C[5] (Štědrá, 2001)	380 ± 3 Ma (Mnz)/metam.
HT-99-7	Ovci Dvur shipyard	medium- to coarse-grained coronitic metagabbro	Pl–Cpx–Hbl–Bt–Ilm–Grt–Ap–Zoi	primary: 16 kbar/900°C[6] Grt corona 600°C[6]	*c.* 500 Ma Timmermann *et al.* (in prep.)
HT-99-8	N of Pistov	garnet-bearing metabasite distinct ~N–S stretching lineation, similar to Münchberg Massif. Maybe older than NW–SE lineation?	Pl, Cpx, Opx–Hbl–Ilm–Grt–Bt–Ap Grt corona 600°C[6]	primary: 16 kbar/900°C[6]	*c.* 500 Ma Timmermann *et al.* (in prep.)
HT-99-9	S-slope of Homolka, quarry	eclogite boudin with strong granulite-facies overprint	Grt–Cpx–Pl–Hbl–Ky–Sil–Spr–Bt–Rt–Ilm–Zrn	14–15 kbar/625–705°C[8]	539 ± 2 Ma (Zrn)/cryst. 377 ± 27 Ma(Zrn, LI)/res., ovg. 349 ± 17 Ma (Rt)/resetting
HT-99-11	roadcut S of Louka,	MORB-type eclogite, boudins in strongly deformed and foliated amphibolite	Omp–Grt–Amp–Ky–Cpx–Pl–Qtz–Rt–Ilm–Ap–Zrn	15·7 kbar/570–640°C[6] 14–16 kbar/625–730°C[7]	382 ± 3 Ma (Zrn)/decomp. >500 Ma (Zrn)/igneous, inh.
HT-99-13	roadcut S of Louka,	retrogressed and strongly deformed amphibolite surrounding eclogite HT-99-11	Act–Pl–Qtz–Ep–Czo–Ttn–Chl–Zrn	9–10 kbar[4]/750°C[3], 8–12 kbar[4]/620–750°C[5] (Štědrá, 2001)	540 ± 9 Ma (Zrn)/cryst. 384 ± 2 Ma (Zrn)/decomp. 365 ± 7 Ma(Ttn)/retr. ~650°C

Štědrá (2001) used [1]GASP barometer of Koziol & Newton (1988), Px barometer of Gasparik & Lindsley (1980), [2]Grt–Cpx thermometer of Powell (1985), [3]Grt–Hbl thermometer of Graham & Powell (1984), [4]barometer of Kohn & Spear (1990), [5]Hbl–Pl thermometer of Blundy & Holland (1994), [6]in Jelínek *et al.* (1997), [7]in Beard *et al.* (1995), [8]in O'Brien (1992). LI, lower intercept age; cryst., crystallization; decomp., decompression; inh., inheritance; metam., metamorphism; ovg., overgrowth; res., resorption; retr., retrograde.

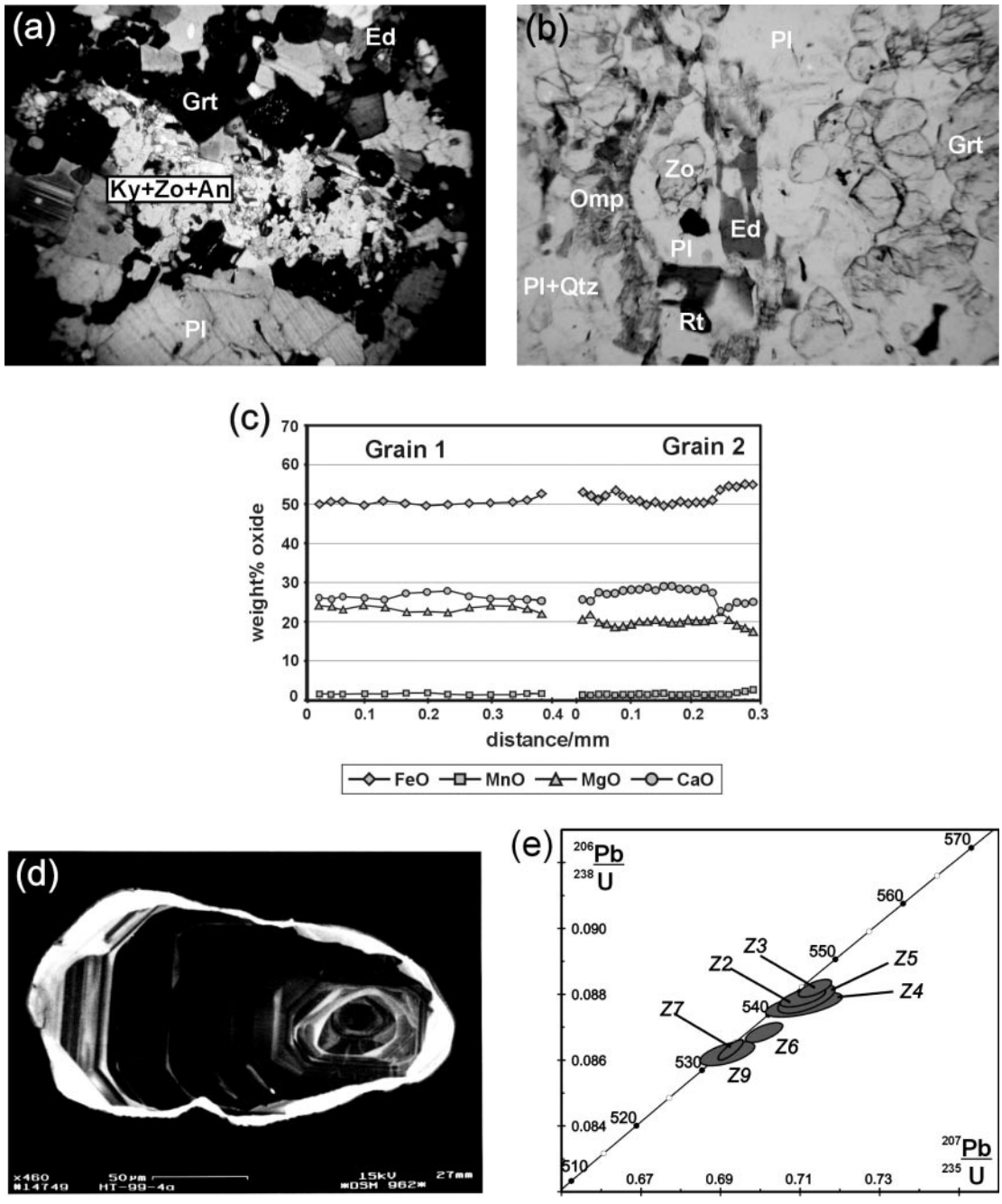

Fig. 2. High-pressure granulite HT-99-4a. (a) Photomicrograph showing aggregate distribution of mineral phases within lighter-coloured, Al-rich domain. In the centre a fine-grained aggregate of relict poikilitic kyanite (Ky) intergrown with zoisite (Zo) and anorthite (An) is surrounded by isometric garnet (Grt, black). An outer zone of coarser-grained plagioclase (Pl; left, bottom) and locally edenite (Ed) separates the Al-rich domain from the darker, garnet-, clinopyroxene-, and amphibole-rich matrix. Crossed polars; length of the field is 2 mm. (b) Photomicrograph of darker, more mafic matrix domains (right and left) that include garnet (Grt), relict omphacite (Omp), plagioclase (Pl), and quartz (Qtz). Contrasting Ca–Al-rich domain in centre comprises zoisite (Zo) as replacement product of kyanite, mantled by granular, recrystallized Ca-plagioclase and subhedral prismatic edenite (Ed). Length of field is 2·2 mm. (c) Compositional traverses through two garnet grains from Al-rich domain. Grain 1 (diameter 0·4 mm) is surrounded by poikilitic kyanite–spinel–anorthite aggregate, grain 2 (diameter 1·2 mm) by kyanite. Compositional zoning in both grains is manifested by grossular-rich cores, increasing almandine and a more variable pyrope component towards the rim, reflecting multi-stage growth. (d) CL image showing small distinct core encircled by overgrowth with oscillatory zoning. 'Layers' of directional (zones becoming progressively finer and non-luminescent towards the rim) oscillatory zoning are separated by thin zones of bright luminescence, which indicate episodic resorption before continuing crystallization. The strongly resorbed grain is surrounded by a highly luminescent, irregular rim that penetrates into the areas of oscillatory zoning. (e) U–Pb concordia diagram showing zircon analyses of sample HT-99-4a overlapping concordia in the interval 545–535 Ma.

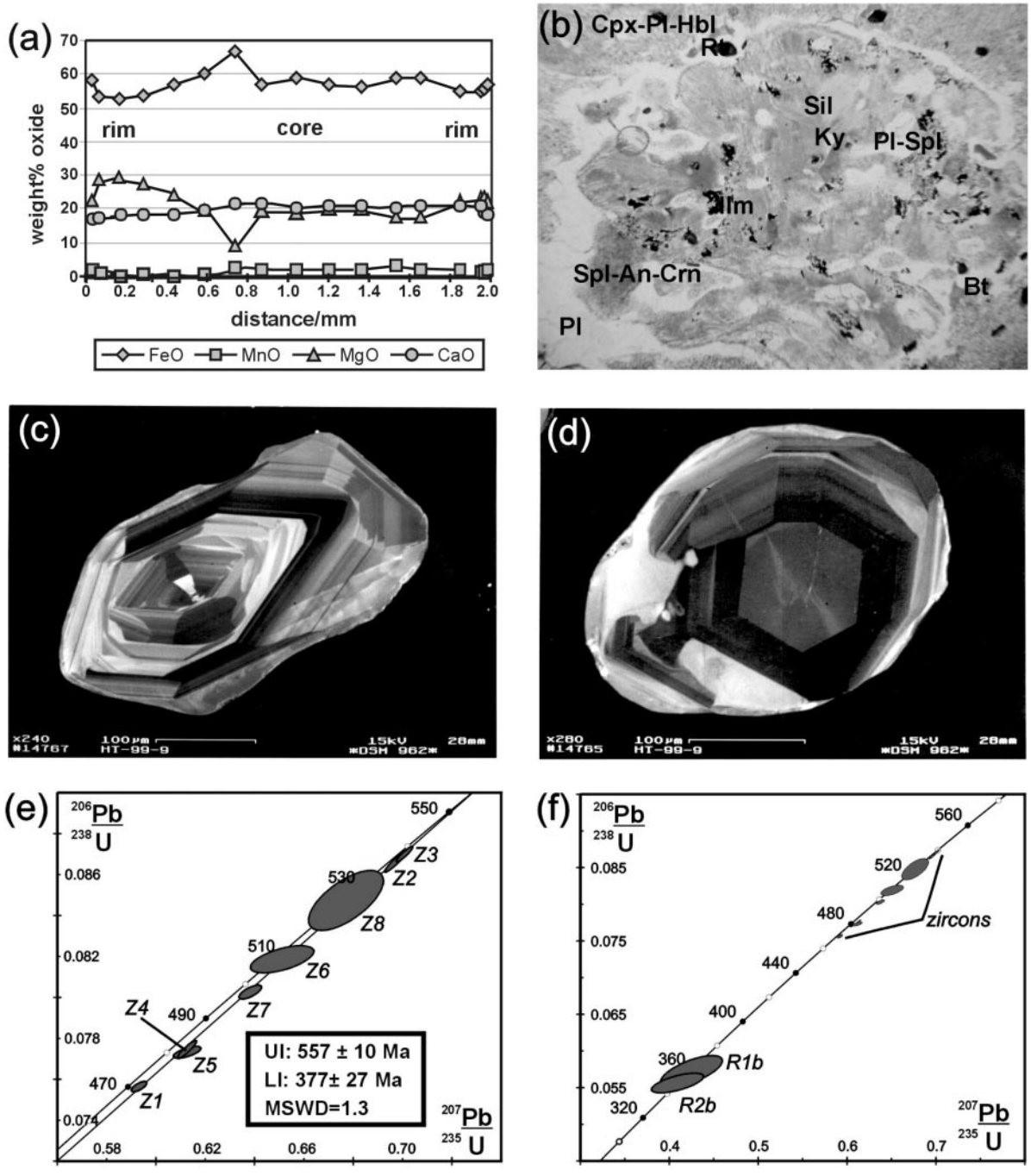

Fig. 3. Eclogite HT-99-9. (a) Compositional profile of garnet (diameter 2 mm) surrounded by a mixture of amphibole, biotite and plagioclase. Compositional plateau in core, then distinct FeO peak (e.g. No. 8), drop of MgO, and slight increase of CaO, representing relicts of strong zoning, should be noted. From here towards the rims FeO decreases and MgO increases, interpreted to reflect heating (granulite-facies overprint?), followed by typical retrograde zoning in the outer rim. (b) Photomicrograph showing relict transparent cores of kyanite (Ky) progressively replaced by fibrous sillimanite (Sil), and towards the rim by somewhat coarser, prismatic corundum (Crn). Fine-grained spinel (Spl)–anorthite (Pl) symplectite in the outer part of the pseudomorph (upper right) is rimmed by a thin corona of Ca-rich plagioclase. Also included in the pseudomorph are bleb-like secondary plagioclase and biotite symplectite. The surrounding matrix is composed of amphibolitized clinopyroxene–plagioclase symplectite (Cpx–Pl–Hbl), zoisite, quartz, and coarse garnet (not shown). Dark grains are rutile and ilmenite. Length of the field is 2 mm. (c) CL image of zircon dominated by pyramid faces exhibiting oscillatory growth zoning and sector zoning in centre and in successive shells. (d) Zircon with homogeneous heptagonal centre surrounded by sector-zoned oscillatory growth, cross-cut by brightly luminescent irregular new zircon growth at the rim. (e) U–Pb concordia diagram showing zircon analyses Z1–Z8 and calculated discordia curve. Low error for analyses Z2 and Z3, which plot near concordia at ≤540 Ma, should be noted. (f) U–Pb diagram showing rutile analyses with respect to zircon analyses. R1b and R2b overlap concordia at *c.* 360 Ma, whereas zircon analyses invariably plot close to the upper intercept shown in (e).

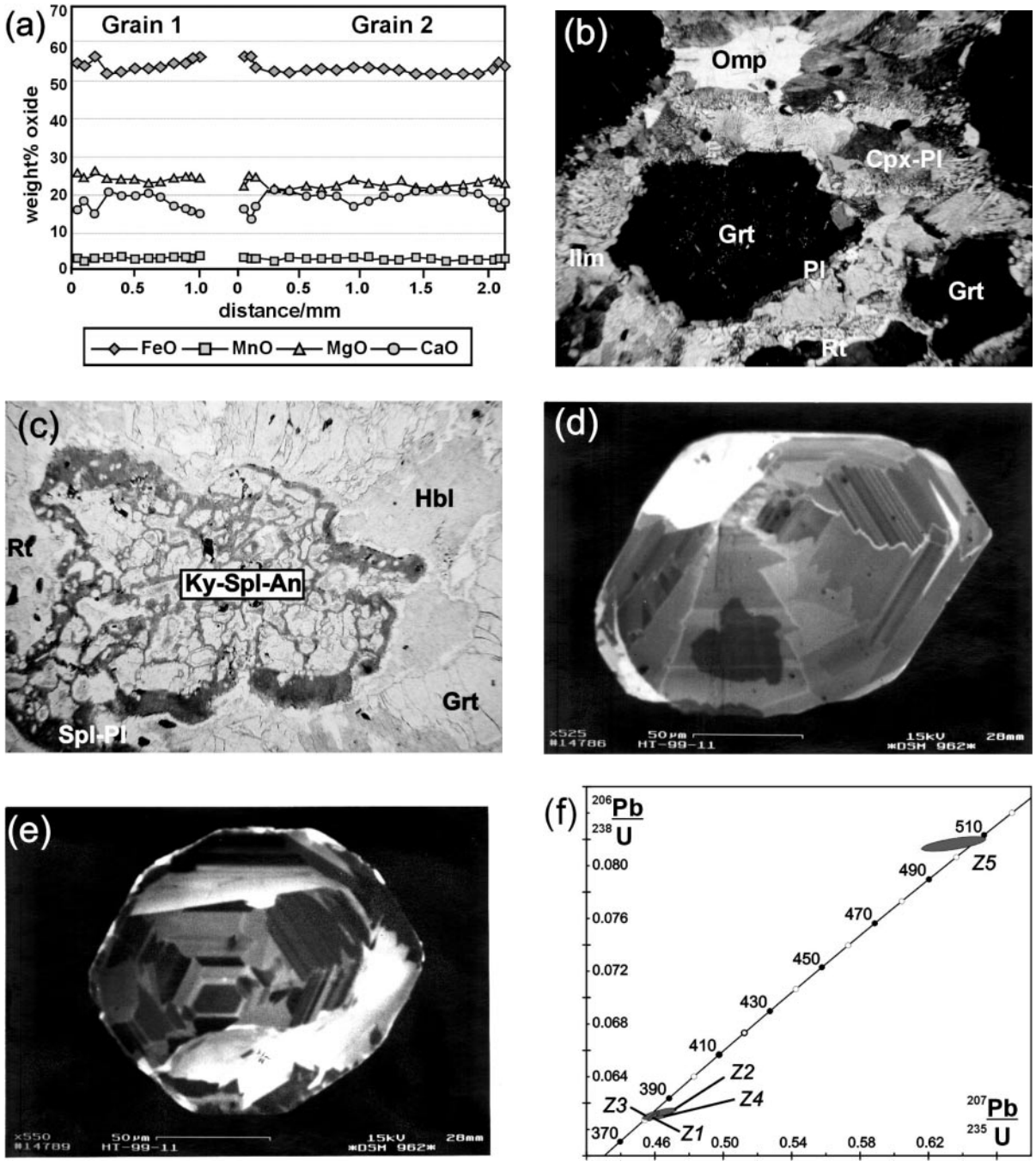

Fig. 4. Eclogite HT-99-11. (a) Compositional profile of two garnet grains (X_{Fe} 0·55–0·60, X_{Mg} 0·21–0·26, X_{Ca} 0·13–0·22, X_{Mn} 0·01–0·02). Grossular component (CaO) decreases, and pyrope (MgO) and almandine (FeO) components increase towards rims (diameter of grain 1 is 1·1 mm; that of grain 2 is 2·2 mm). (b) Decompression texture in eclogite: garnet (Grt) porphyroblast (in black) is rimmed by narrow corona of plagioclase (Pl) and matrix of vermicular aggregates of clinopyroxene–plagioclase (Cpx–Pl) symplectite and minor quartz. Reduction of symplectites towards relict omphacite core (bright grain in upper left) without recrystallization indicates continuous pressure decrease and minimal thermal effect. Dark grains are rutile and ilmenite. Crossed polars; length of field is 2·2 mm. (c) Poikilitic kyanite (Ky) includes small globular symplectitic aggregates of plagioclase–omphacite and plagioclase–biotite, garnet and rutile. Conspicuous spinel–plagioclase (Spl–Pl) corona (high relief) rims both outer and inner kyanite contacts to Fe–Mg-bearing phases. Large irregular cracked grains in the upper and lower right field are garnet (Grt); the remaining light grey matrix consists of amphibolitized fine-grained clinopyroxene–plagioclase symplectite. Plane-polarized light; length of field is 2 mm. (d) CL image showing radiating growth of 'fir-tree' sector zoning from the upper left part of the zircon. An irregular brightly luminescent patch in the upper left corner of the grain overprints the initial sector zoning. (e) Small homogeneous dark hexagonal centre surrounded by sector zoning (mainly 'fir-tree' zoning) of distinctly different luminescence. Recrystallization in rim areas is manifested by irregular bright luminescent patches. (f) U–Pb diagram showing zircon analyses of sample HT-99-11.

grains are mostly pale and inclusion-free, similar to rims of larger grains. Garnet and relict omphacite (up to 2 mm; X_{Jd} ~42–46) are surrounded by diopside (X_{Jd} 0·20–0·26)–plagioclase (X_{Ab} 0·10) symplectite and fine vermicular symplectite (Fig. 4b). Enstatite and albite symplectites, in contact with garnet and clinopyroxene, are less common. Poikiloblastic kyanite is replaced by anorthite and spinel (Fig. 4c).

Sample HT-99-13 is from a strongly foliated, fine-grained, dark grey–green amphibolite wrapping around the above eclogite boudin HT-99-11. Olive–green hornblende occurs in poikilitic aggregates intergrown with plagioclase, possibly replacing weakly globularized symplectite after a high-pressure phase of clinopyroxene. The rounded shape of the plagioclase and amphibole clusters indicates replacement of former garnet porphyroblasts from eclogite (Fig. 5a). Amphibole–plagioclase aggregates are surrounded by later generation blue–green prismatic amphibole (± plagioclase). Small subhedral to euhedral titanite is aligned along the schistosity.

Sample HT-99-6, derived from a deformed orthogneiss body in the northwestern MLC, is a medium- to coarse-grained mylonitic gneiss with a strong linear fabric, along which the feldspar and quartz grains are extended (Fig. 6a). Relict feldspar porphyroclasts with oval quartz inclusions are surrounded by anastomosing ribbons of recrystallized quartz and plagioclase. Feldspar porphyroclasts locally contain foliation-parallel 'book-shelf' cracks filled by late Fe-chlorite. Sparse biotite flakes are disseminated in the matrix; these occur in discontinuous bands that show a preferred orientation, or form intrafoliation fishes along microshear surfaces.

Sample HT-99-1 is a felsic leucosome in a boudin neck of the mafic host rock of the MLC (Fig. 7a). The medium- to fine-grained matrix consists mostly of quartz and plagioclase (andesine to labradorite) with a weak preferred orientation. Xenoblastic calcic amphibole and oligoclase form irregular aggregates along quartz ribbons. Subordinate, partly chloritized, anhedral garnet shows a weak compositional variation. Relict kyanite laths (≤5 mm) between quartz ribbons and matrix are replaced by fine-grained muscovite and pyrophyllite (Fig. 7b). In recrystallized domains, coarse, fan-shaped mica laths are surrounded by fine-grained muscovite.

Coarse-grained, coronitic metagabbro HT-99-7 and pale grey, medium-grained metagabbro HT-99-8 are both part of a metagabbro suite in the southeastern MLC at the TBU boundary. The metagabbros exhibit a relict ophitic to coronitic texture with metamorphic garnet surrounding clinopyroxene, amphibole and ilmenite. Well-preserved magmatic plagioclase is partly recrystallized and dusted by tiny needle-shaped kyanite, zoisite, or pseudomorphs of anorthite after zoisite (Štědrá, 2001). In HT-99-8, relict, colourless orthopyroxene occurs in the centre of clinopyroxene–biotite–hornblende aggregates. Although metamorphic kyanite may occur, equilibrated high-pressure minerals, such as Na-rich clinopyroxene/omphacite, are absent.

GEOCHEMISTRY

For characterization and comparison with previous data (Beard *et al.*, 1995), we analysed samples HT-99-4a, HT-99-8, HT-99-9 and HT-99-11 for major and trace element concentrations, samples HT-99-1, HT-99-7 and HT-99-13 for trace element concentrations (Table 2a and b, Fig. 8), and the Rb–Sr and Sm–Nd isotope ratios of all samples (Table 3, Fig. 9).

The metabasic rocks of the MLC have high Y/Nb ratios (>2) typical for tholeiitic or calc-alkaline basalts. Except for metagabbro HT-99-7, they fall along a tholeiitic differentiation trend (Fig. 8a). Eclogites HT-99-9 and HT-99-11, with Mg numbers (Table 2a) of 54–59, high Cr and Ni, εNd values of 6·8–7·7, and a chondrite-normalized Nd/Sm ratio around 1·1, represent the most primitive compositions of our MLC samples. The two eclogites are compositionally similar to those studied by Beard *et al.* (1995; εNd_{T500} = 5–10, Mg numbers = 48–72), the latter having variably depleted to flat (rarely LREE-enriched), REE patterns ($[Ce/Yb]_{chon}$ = 0·23–1·1). HT-99-9 and HT-99-11 have large ion lithophile element (LILE), Rb, K, Ba, and Sr contents, Sr/Rb ratios (35–66), K/Ba ratios (22–40), and Zr/Rb ratios (14–21) that are similar to somewhat enriched MORB and island arc tholeiites (IAT; Fig. 8b; e.g. Pearce, 1983; Humphris *et al.*, 1985). The LILE contents, however, may have been altered as a result of element mobility during high-grade metamorphism.

Metagabbro HT-99-8 is characterized by a high Mg number (59) and high Cr content. Compared with the eclogites, the $[Nd/Sm]_{chon}$ (1·2–1·3) and LILE concentrations are somewhat higher (Fig. 8b), whereas εNd values (4·6–4·9), Sr/Rb ratios (17–29), and Zr/Rb ratios (7–8) are somewhat lower. High-pressure granulite HT-99-4a has a more evolved composition, with low Ni, Cr, Mg number (36), and εNd (2·9), as well as a pronounced LREE enrichment ($[Nd/Sm]_{chon}$ of 1·6). Furthermore, HT-99-4a has low Y contents, a Sr/Y ratio of 53, a Zr/Sm ratio of 120, and high Al_2O_3 contents. Amphibolite HT-99-13, although spatially closely associated with eclogite HT-99-11, has a distinct trace element and isotope composition with remarkably low Sm, Nd, Rb, and Sr contents (Fig. 8). The $[Nd/Sm]_{chon}$ and Sr/Rb ratios (40) are similar to those of the metagabbros, although Zr/Rb (50) is higher and εNd lower (2·5). Leucosome HT-99-1 has the highest $[Nd/Sm]_{chon}$ of all samples (1·9) and an isotope composition close to those of HT-99-13 and HT-99-4a. Compared with the metagabbros, the orthogneiss is enriched in LILE and depleted in transition elements (e.g. Cr, Ni, Zn), Nb, and Y.

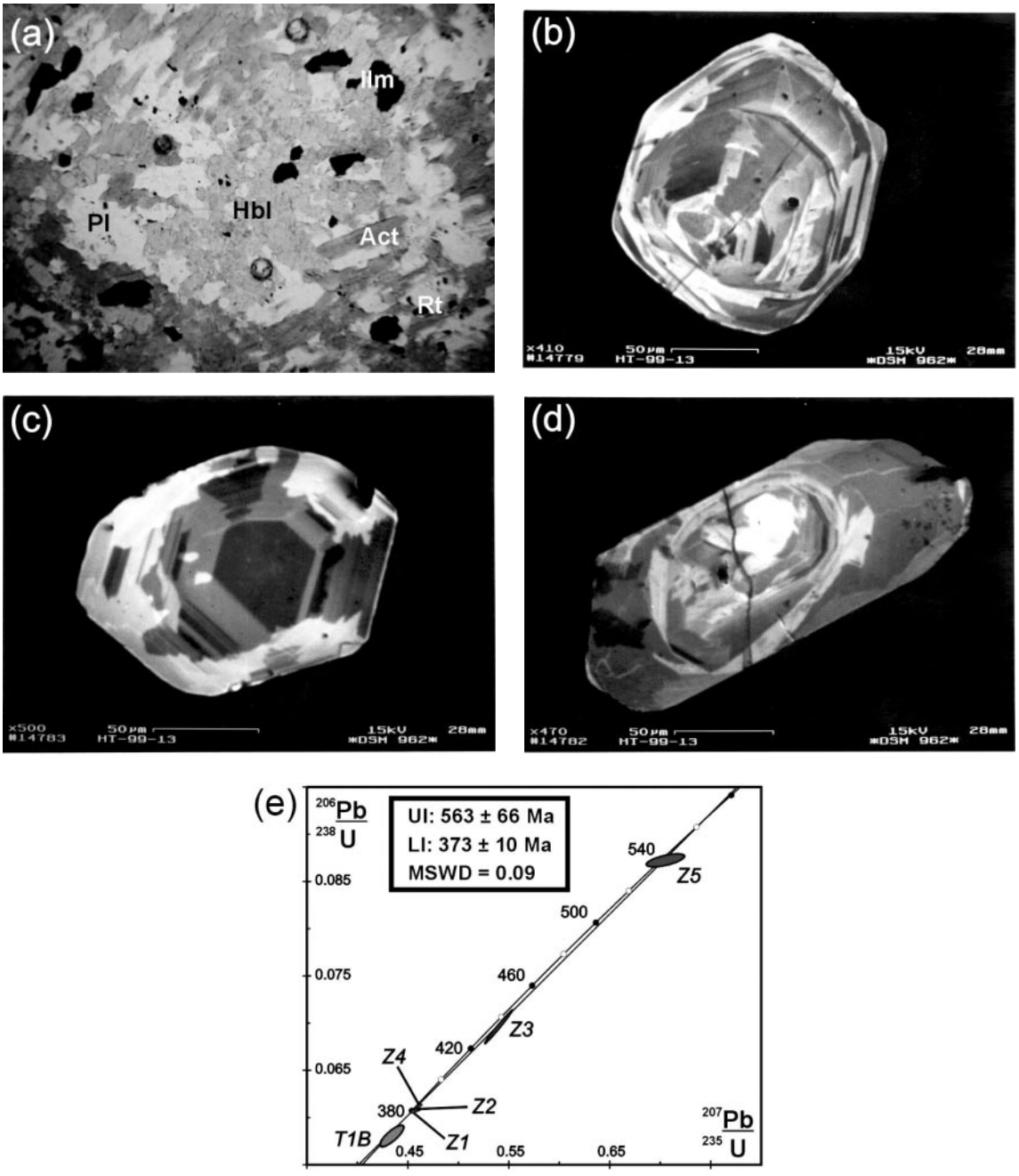

Fig. 5. Amphibolite HT-99-13. (a) Photomicrograph showing recrystallized matrix of plagioclase (Pl), hornblende (Hbl), ilmenite (Ilm), and rutile (Rt). The suboval aggregate in the centre has a higher content of recrystallized plagioclase than the matrix and is surrounded in places by actinolitic amphibole (Act), indicating replacement of former garnet porphyroblasts (from eclogite?) or plagioclase. Plane-polarized light; length of field is 2·2 mm. (b) CL image of round and multifaceted zircon grain with internal 'fir-tree' sector zoning, locally with overprint of brightly luminescent 'schlieren' in rim areas. (c) Multifaceted zircon with homogeneous, non-luminescent centre and surrounding planar growth banding and 'fir-tree' sector zoning reveal irregular, highly luminescent patches in rim areas. (d) Centre part of prismatic zircon with small bright centre and surrounding planar growth zoning is cut off by rim of bright luminescence, followed by only weakly luminescent radial sector-zoned growth (Vavra *et al.*, 1996). (e) U–Pb diagram showing zircon and titanite analyses of sample HT-99-13.

In a $^{87}Sr/^{86}Sr$–εNd diagram (Fig. 9), the mafic samples analysed in this study and most previous data from Beard *et al.* (1995) form an array with strong variations of εNd values compared with the majority of Sr isotope compositions. This suggests the absence of post-magmatic disturbance of the isotope systems. Exceptions are the variably enriched $^{87}Sr/^{86}Sr_{T500}$ ratios for some eclogites from Beard *et al.* (1995; Fig. 9), which those workers

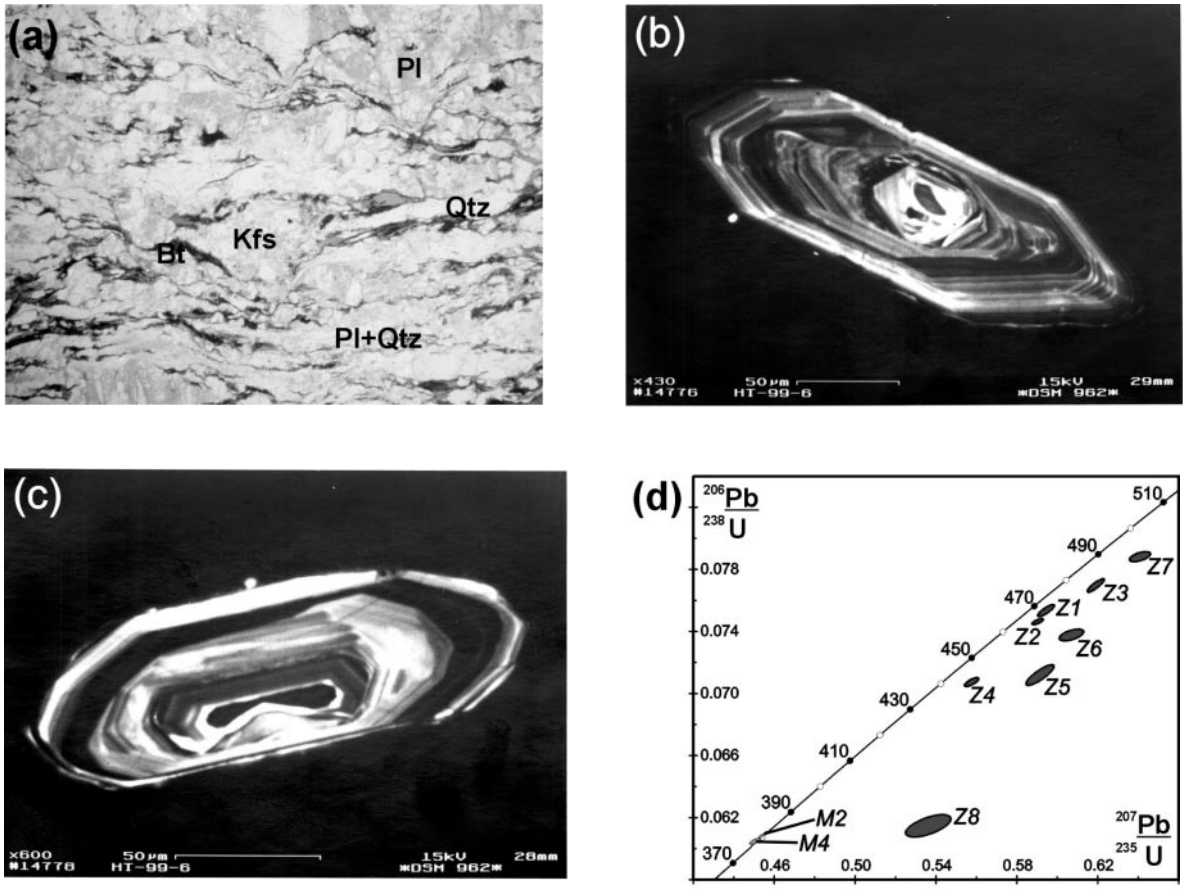

Fig. 6. Orthogneiss HT-99-6. (a) Thin section showing relict feldspar porphyroclasts in reworked matrix with linear to planolinear deformation. Length of field is 1 cm. (b, c) CL images showing complex zoning patterns and cores in the orthogneiss zircons. Luminescent cores (b) are surrounded by darker planar growth zoning (b) or sector zoning (c). The conspicuous resorption of core (c) or middle area (b) should be noted. In some grains, outer zircon layers are characterized by highly luminescent (c), oscillatory zoning (b, c). (d) U–Pb diagram showing distribution of discordant zircon analyses and concordant monazite analyses at 380 Ma.

explained by seawater alteration. In contrast, felsic orthogneiss HT-99-6 has an elevated $[Nd/Sm]_{chon}$ ratio (1·5) and an εNd(t) value of –2·3. Although the $^{87}Sr/^{86}Sr_{T500}$ ratio (0·711) is high, the orthogneiss still falls in the field of Pre-Mesozoic European crust (Gerdes *et al.*, 2000).

ZIRCON TEXTURES AND RESULTS OF U–Pb GEOCHRONOLOGY

Zircon is a common accessory mineral in high-pressure granulite HT-99-4a, mainly in the plagioclase-rich areas, where zircon grains are rarely associated with poikiloblastic garnet. The zircon grains have different morphologies, such as long-prismatic, short-prismatic, isometric, and oval to round; in many cases they have microscopically visible cores. Resorption of the grains is common, resulting in 'dogbone' zircon; these are typical products of incomplete dissolution in a partial melt that is successively extracted to produce restitic granulite-facies rocks (e.g. Vavra *et al.*, 1996). Typical cathodoluminescence (CL) images of the zircon grains show complex textures, mostly with oscillatory zoning (Fig. 2d), which reflect igneous crystallization (e.g. Pidgeon, 1992). Rims of variable width consist of homogeneous, unzoned zircon, that appears highly luminescent in the CL images and is typical for resorption by melt and precipitation of new zircon (e.g. van Breemen *et al.*, 1987). U–Pb zircon analyses of mostly single zircon grains of the different morphologies (described above) yield concordant and nearly concordant error ellipses that overlap with the concordia in the interval 545–535 Ma (Fig. 2e, Table 4).

Eclogite HT-99-9 contains zircon that is generally very clear and of prismatic to isometric habit; an oval to round or multifaceted habit is more rare. Resorption is common, but less so than observed in sample HT-99-4a. CL images (Fig. 3c) reveal oscillatory zoning within zircon grains dominated by pyramid faces. Euhedral, bipyramidal cores are surrounded by both sector- and oscillatory zoned shells of similar habit. Sector zoning results from a

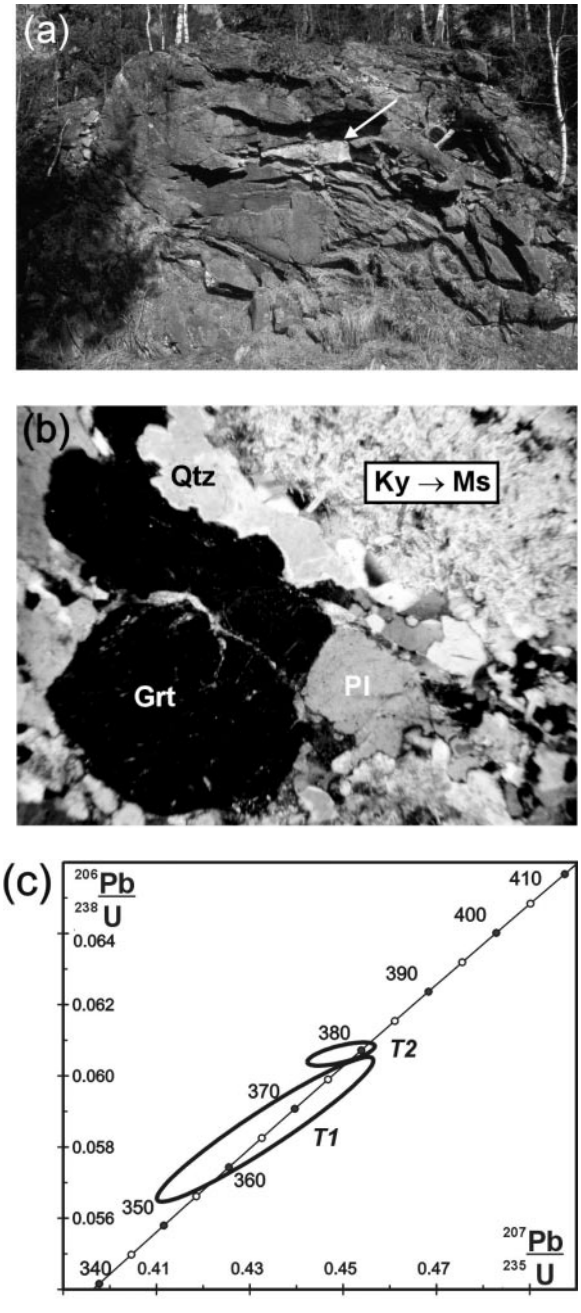

Fig. 7. Leucosome HT-99-1 (a) Field locality with outcrop showing light, felsic Pl–Qtz-rich remobilizate (centre, see arrow) in neck of mafic boudin. (b) Photomicrograph showing texture of kyanite (Ky) replacement by muscovite (Ms; upper right corner) in a matrix of garnet (Grt; X_{Fe} 0·6–0·66, X_{Mg} 0·09–0·15, X_{Ca} 0·21–0·24, X_{Mn} 0·01–0·05), plagioclase (Pl), and quartz (Qtz). (c) Open error ellipses in U–Pb concordia diagram reflect titanite analyses T1 and T2 (Table 2).

variable distribution of trace elements (U, Th, REE) in the pyramidal and prismatic faces of zircon during crystallization (Vavra, 1989). At the rims, brightly luminescent unzoned zircon obliterating the pre-existing zoning (Fig. 3d), is generally due to resorption by melt followed by reprecipitation of new zircon (e.g. van Breemen *et al.*, 1987; Pidgeon, 1992). Eight single- to multigrain zircon fractions of the various morphologies of this sample analysed for U–Pb geochronology are variably discordant from 0·4 to 5·3% (Fig. 3e, Table 4). Single-grain oval zircons Z2 and Z3 yield the most concordant ages of *c.* 537 ± 3 Ma and 539 ± 2 Ma, respectively. The concordance of these grains is due to the fact that abrasion works more efficiently on oval or round morphologies than on (long-) prismatic morphologies, the predominant habit of the other analysed zircon grains from this sample. Thus, more of the thin outer rim of younger growth was removed from round or oval grains, which led to reduction or even elimination of discordance (e.g. Timmermann *et al.*, 2002). Regression of all eight zircon analyses gives an upper intercept age of 557 ± 10 Ma and a lower intercept age of 377 ± 27 Ma. The upper intercept age overlaps, within error, with the nearly concordant ages of Z2 and Z3, suggesting protolith crystallization around 539 Ma. The lower intercept age of 377 Ma is interpreted to reflect the metamorphic/anatectic event during which the protolithic zircon experienced resorption and new growth at the rim (e.g. Fig. 3d). In addition, two xenomorphic, red–brown multigrain rutile fractions were analysed. The analyses have moderately high errors, but the ellipses overlap the concordia at about 360 Ma (Fig. 3f).

Zircon crystals from eclogite HT-99-11 are very clear, with short-prismatic, equant, oval, or round morphologies; long-prismatic zircon is rare. In thin section, the zircon grains mainly occur in or next to hornblende, also within the pale margins of garnet. CL images show zircon grains with homogeneous, weak to nonluminescent centres surrounded by sectors of differential luminescence and internal growth banding (Fig. 4d and e). The most common type of sector zoning observed in zircon grains from this sample is the 'fir-tree' variety, i.e. those with zigzag boundaries between the different growth sectors (Fig. 4d). The 'fir-tree' zoning indicates fluctuating growth rates of individual crystal faces and fast growth at high cooling rates (Vavra *et al.*, 1996). The imaged zircon grains (Fig. 4d and e) also show very bright discordant patches overprinting the initial sector zoning at or near the zircon rim, and indicate a late phase of zircon recrystallization. U–Pb analyses of four single- and multigrain fractions (short-prismatic Z1, round and multifaceted Z2, oval Z3, oval Z4) are concordant, with error ellipses overlapping concordia at *c.* 382 Ma (Fig. 4g, Table 4). Analyses Z2 and Z4 have large $^{207}Pb/^{206}Pb$ errors compared with those for the Pb/U ages, this being due to very small amounts of radiogenic Pb within the zircon grains from this eclogite (Table 4). The concordant age of 382 ± 3 Ma (Z1, Z3) is interpreted to reflect growth of 'fir-tree' sector-zoned zircon. Only reverse

Table 2a: XRF—major element concentrations (in %) of whole-rock samples, MLC

Sample no.	SiO_2	TiO_2	Al_2O_3	FeO*	MnO	MgO	CaO	Na_2O	K_2O	P_2O_5	Sum	Mg no.
HT-99 4a	53·3	1·61	20·5	9·09	0·16	2·57	6·53	4·64	0·22	0·38	99·4	33·5
HT-99-8	50·6	1·30	17·7	8·21	0·14	6·53	10·2	3·28	0·67	0·16	98·8	58·7
HT-99-9	48·3	1·37	18·8	10·4	0·19	6·93	9·82	2·76	0·12	0·29	99·0	54·2
HT-99-11	48·6	1·37	17·2	10·2	0·19	8·15	9·88	3·41	0·20	0·17	99·3	58·8

*Total iron as FeO.
Sum is total without H_2O and CO_2. Mg number = [molecular Mg/(Mg + Fe_{tot})] × 100.

Table 2b: XRF—trace element concentrations (in ppm) of whole-rock samples, MLC

Sample no.	Y	Zr	Nb	Ni	Cu	Zn	Ga	Pb	Th	Ba	V	Cr	Sr/Rb	K/Ba	Zr/Rb	Sm/Nd*	Sr/Y	Y/Nb
HT-99-1	8	112	LL	LL	LL	10	13	15	16	212	26	5	18·5	—	4·0	1·93	64	—
HT-99-4a	14	360	LL	LL	11	96	23	8	LL	183	104	18	302	10·0	148	1·55	53	—
HT-99-7	19	92	8	16	LL	58	19	LL	LL	129	130	45	29·2	—	8·3	1·24	17	2·4
HT-99-8	27	105	5	34	25	66	20	6	LL	197	161	249	17·4	28·2	7·1	1·32	10	5·4
HT-99-9	16	87	6	85	105	100	20	LL	LL	25	289	202	65·5	40·0	21·2	1·15	17	2·7
HT-99-11	28	77	LL	131	14	86	17	6	LL	74	234	283	35·0	22·3	13·5	1·09	7	—
HT-99-13	31	116	9	81	25	100	18	5	LL	58	272	116	50·3	—	43·0	1·26	4	3·4

LL, lower detection limit (<5 ppm for Nb, Pb, Th; <10 ppm for Cr, Ni, Cu, Zn).
*Chondrite-normalized ratio.

discordant analysis Z5 (long-prismatic zircon fragment) is older, with U/Pb ages around 500 Ma (Fig. 4f, Table 4).

The amphibolite HT-99-13 contains very clear, short-prismatic to isometric, or oval to round (± multifaceted), zircon with some resorption features. CL images exhibit different patterns of sector zoning, including 'fir-tree' zoning, within the grains (Fig. 5b and c). The zoning is commonly overprinted by irregular, unzoned, bright luminescent patches or rims that may have formed during late recrystallization (e.g. Pidgeon, 1992). Some zircon grains have inherited cores, surrounded by sector zoning and/or planar growth zoning (Fig. 5d). U–Pb analyses of single- and multigrain fractions Z1 (cloudy fragment), Z2 (three short-prismatic, stubby grains), and Z4 (seven prismatic grains, *c.* ≥2:1) give concordant ages around 384 ± 2 Ma. In contrast, U–Pb analysis of single zircon Z5 (prismatic, slightly cloudy, inclusions) is concordant at 540 ± 9 Ma, and has a distinctly higher U content compared with the other, younger fractions (Fig. 5f, Table 4). Only multigrain fraction Z3 (eight small, short-prismatic grains) is discordant with a $^{207}Pb/^{206}$ Pb age of 454 ± 7 Ma. A regression line calculated on the basis of all of the analysed zircon fractions (MSWD = 0·088; Fig. 5e) yields an upper intercept age of 563 ± 66 Ma, which overlaps within error with the more precise age of *c.* 540 Ma from zircon Z5. The 540 Ma age is taken to reflect initial zircon growth during protolith crystallization (e.g. Fig. 5d). The lower intercept age of 373 ± 10 Ma agrees with the more precise concordant 384–380 Ma zircon ages of fractions Z1, Z2, and Z4. Analysis Z3, falling on the regression line, is interpreted to represent a mixture of *c.* 540 Ma protolithic zircon and a *c.* 380 Ma component. One multigrain fraction of coarse (≥250 μm), dark brown, titanite was analysed, giving a concordant age of 365 ± 7 Ma (Fig. 5e; Table 4). This age is taken to reflect the timing of the strong retrogression within the amphibolites.

The orthogneiss HT-99-6 predominantly contains long- to short-prismatic bipyramidal zircon grains (± inclusions) typical of a magmatic origin (e.g. Pupin, 1980). Oval to round, multifaceted zircon crystals are rare. CL images reveal complex internal structures, such as distinct cores with oscillatory or patchy zoning surrounded by zircon with planar growth zoning or sector zoning (Fig. 6b and c). The middle zone in the zircon grains is often resorbed and typically surrounded by rims showing oscillatory zoning ranging from very bright to very dark luminescence. The complex patterns within these grains are reflected in the invariably discordant U–Pb analyses of the single- and multigrain zircon fractions, with $^{207}Pb/^{206}Pb$ ages ranging from 716 ± 29 Ma to 498 ± 8 Ma (Fig. 6d, Table 4). The spread of the error

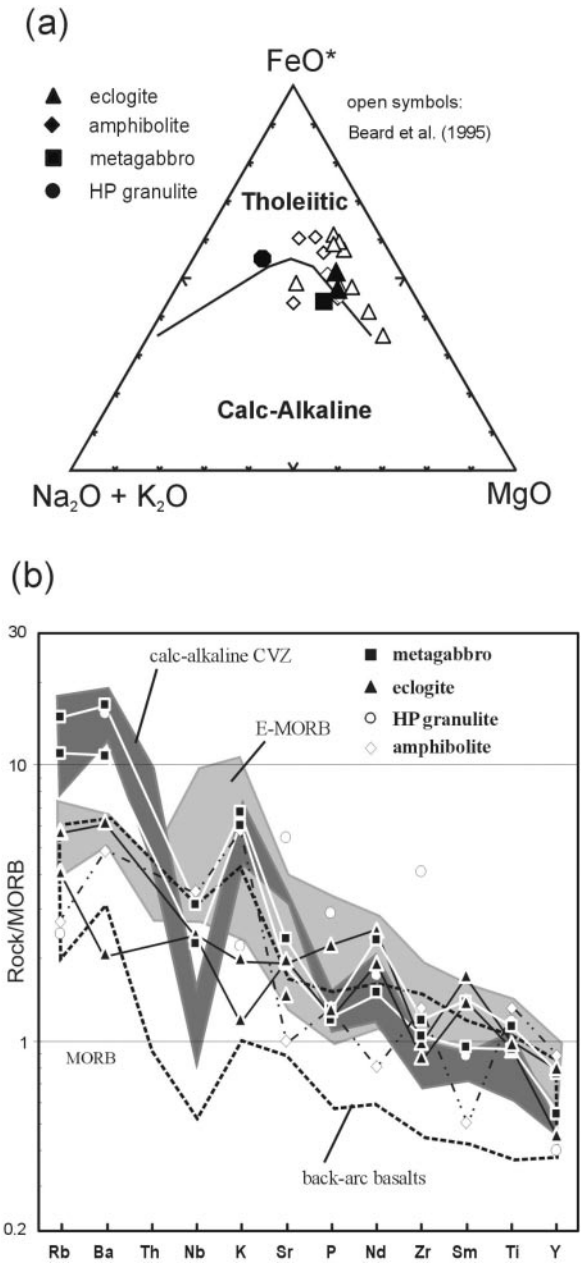

Fig. 8. Chemical variation and discrimination diagrams for mafic rocks from the MLC. (a) AFM plot after Irvine & Baragar (1971) discriminating tholeiitic and calc-alkaline chemistries. (b) MORB-normalized (Hofmann, 1988) trace element variation diagram. The fields of back-arc basalts (Saunders & Tarney, 1979), enriched (E-) MORB (Humphris *et al.*, 1985; Le Roex *et al.*, 1985), and calc-alkaline rocks from the Central Volcanic Zone (CVZ) of the Andes (Hickey *et al.*, 1986) are for comparison.

ellipses cannot be correlated by regressing all or some of the U–Pb analyses. Instead, any regression curve attempted passes through only one or a few ellipses with a very high MSWD. We interpret this as inheritance of the zircon cores and various subsequent overgrowth events, one of which being crystallization of the present orthogneiss. The heavy mineral separate (0·4 amp fraction) of this sample also contained few small, rounded, greenish yellow monazite grains. Single-grain fraction M2 (euhedral, fractured, very slightly cloudy, tiny inclusions) and multigrain fraction M4 (three clear, yellowish euhedral grains ± inclusions) yield concordant ages of 380 ± 3 Ma (Fig. 6e, Table 4).

Leucosome HT-99-1 contains only a very low modal abundance of zircon of various morphologies. These include oval to round grains with internal 'fir-tree' sector zoning. In contrast, long-prismatic zircon crystals have distinct (zoned) cores, with variably wide 'fir-tree' sector-zoned overgrowths at the pyramidal terminations. Titanite, as part of the newly crystallized assemblage, is used to determine the age of anatexis and remobilization of the basic host rock. Two yellowish brown to dark brown multigrain titanite fractions are slightly reverse discordant, but the error ellipses still overlap concordia (Fig. 7c) at 366 ± 13 Ma (T1) and 378 ± 4 Ma (T2).

DISCUSSION

Interpretation of geochronological data and geochemistry

The eclogites of the MLC (Beard *et al.*, 1995; this study) have an elemental and isotope composition that ranges between normal to slightly fractionated and enriched ocean-floor basalt (E-MORB). In particular, the LILE and REE contents of HT-99-9 and HT-99-11 are more typical of E- or T- (transitional) type MORB (Le Roex *et al.*, 1985). Some back-arc tholeiites have comparable trace-element patterns (Saunders & Tarney, 1979), but such rocks tend to show characteristic depletion in high field strength elements (HFSE). The eclogitic protoliths, however, could also be mafic magmas that intruded at the base of, or into, continental crust, although such rocks are usually characterized by a more enriched isotope composition than the MLC eclogites as a result of crustal contamination. They could be derived from a less depleted or even slightly enriched source, with or without crustal contamination (e.g. Hawkesworth & Vollmer, 1979; Hawkesworth *et al.*, 1990; Voshage *et al.*, 1990).

Petrographic observations, internal zircon structures, and the fairly high Th/U ratios in zircon of eclogite HT-99-9 indicate igneous crystallization, probably as a gabbro, at 539 ± 2 Ma. The chemical and isotopic compositions of both the studied eclogites are similar, and a common origin, and therefore similar protolith age, seems likely. However, eclogite HT-99-11 does not contain *c.* 540 Ma zircons. Although the older (*c.* 500 Ma), more U-rich zircon in eclogite HT-99-11 may relate to protolith crystallization, we also consider the possibility that this inheritance originates from adjacent rock units. One possible explanation for the absence of 540 Ma ages

Table 3: Whole-rock Sm–Nd and Rb–Sr concentrations and $^{143}Nd/^{144}Nd$ and $^{87}Sr/^{86}Sr$ isotope compositions

Sample no.	Sm (ppm)	Nd (ppm)	$^{147}Sm/^{144}Nd$	$^{143}Nd/^{144}Nd^{*}$	$^{143}Nd/^{144}Nd_{(500)}$	εNd (500)	Rb (ppm)	Sr (ppm)	$^{87}Rb/^{86}Sr$	$^{87}Sr/^{86}Sr^{*}$	$^{87}Sr/^{86}Sr_{(500)}$
HT-99-1	2·54	15·1	0·1016	0·512443 ± 3	0·512110	2·3	27·8	513	0·1566	0·70501 ± 1	0·70450
HT-99-4a	2·91	13·9	0·1266	0·512557 ± 3	0·512142	2·9	2·4	737	0·0096	0·70404 ± 1	0·70400
HT-99-6	2·69	12·2	0·1337	0·512316 ± 3	0·511878	−2·3	96·8	181	1·548	0·71624 ± 1	0·71117
HT-99-7	3·15	12·0	0·1592	0·512766 ± 3	0·512245	4·9	11·0	320	0·0990	0·70381 ± 1	0·70349
HT-99-8	4·58	18·6	0·1488	0·512716 ± 3	0·512228	4·6	14·8	258	0·1660	0·70413 ± 1	0·70358
HT-99-9	5·70	20·1	0·1715	0·512903 ± 3	0·512341	6·8	4·1	267	0·0441	0·70396 ± 1	0·70382
HT-99-11	4·58	15·3	0·1828	0·512988 ± 3	0·512389	7·7	5·7	200	0·0827	0·70392 ± 1	0·70365
HT-99-13	1·67	6·47	0·1558	0·512632 ± 3	0·512122	2·5	2·7	136	0·0575	0·70424 ± 1	0·70405

*Measured ratio.
Errors are 1σ and refer to least significant digit(s); (500) indicates initial ratio at 500 Ma.

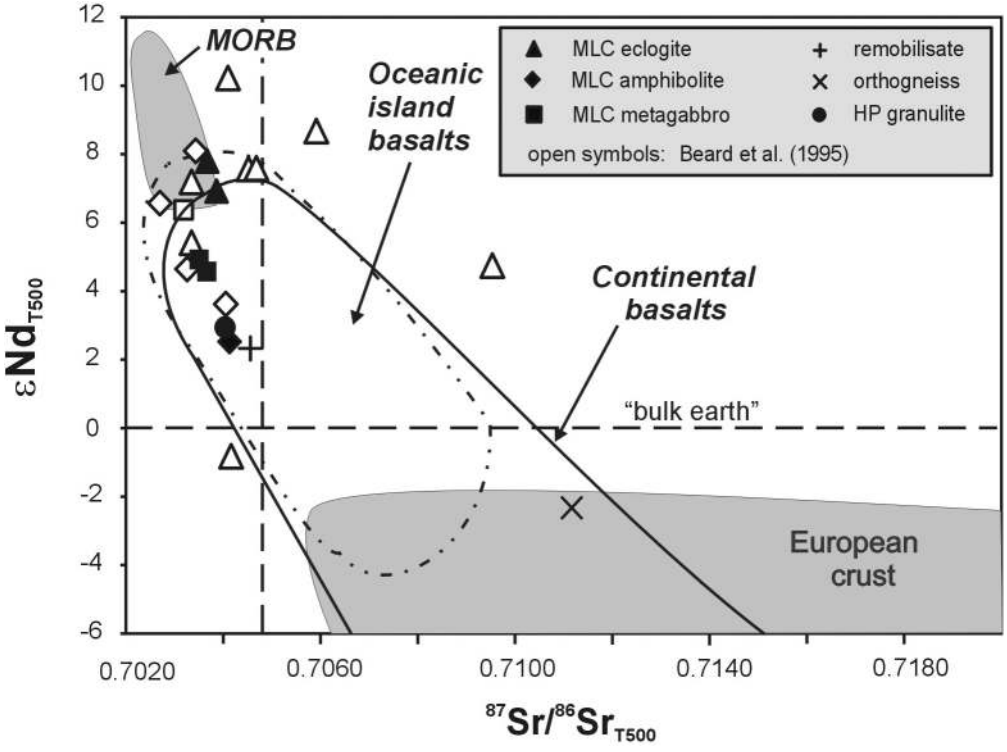

Fig. 9. εNd_{T500} vs $^{87}Sr/^{86}Sr_{T500}$ of samples from the MLC [open symbols from Beard *et al.* (1995)]. Schematic ocean-island basalt and continental basalt fields after White (1999). Present-day MORB field after Taylor *et al.* (1997) and Kempton *et al.* (2002). It should be noted that the MORB field was probably about 1 εNd unit lower at 0·5 Ga. Pre-Mesozoic European crust after Gerdes *et al.* (2000).

is that the protolith was a basalt with MORB affinity that did not crystallize protolithic zircon. Concordant zircon in HT-99-11 formed as late as 382 ± 3 Ma, contemporaneous with the Variscan event of crustal stacking and regional metamorphism in this area (e.g. Zulauf, 1997*b*; Dörr *et al.*, 1998; Table 5b). The 'fir-tree' structures in HT-99-11 zircons are typical zoning patterns reflecting fast growth under upper amphibolite-facies to granulite-facies conditions and are generally interpreted to form on the retrograde *P–T* path in the presence of melt (Vavra *et al.*, 1996, 1999; Schmitz & Bowring, 2000). Zr must have been released from other minerals, such as pyroxene and amphibole (e.g. Fraser *et al.* 1997; Schmitz & Bowring, 2000), to facilitate zircon growth for the first

Table 4: U–Pb zircon, monazite, titanite, and rutile data, MLC, Czech Republic

Sample, fraction[1]	Wt.[2] (mg)	U (ppm)	Pb[3] (ppm)	$^{206}Pb/^{204}Pb$[4]	Pb[5] (pg)	Th/U[6]	$^{206}Pb/^{238}U$[7]	$^{207}Pb/^{235}U$[7]	$^{207}Pb/^{206}Pb$[7]	$^{206}Pb/^{238}U$[8] (Ma)	$^{207}Pb/^{235}U$[8] (Ma)	Corr. coeff.	$^{207}Pb/^{206}Pb$[8] (Ma)	Disc.[8] (%)
HT-99-4al; HP granulite, Otrocin Valley (5548961, 3346687)[9]														
Z2 (*1*;c,p,i)	0·0029	139·5	11·95	620	3·64	0·2396	0·08793 ± 0·20	0·7113 ± 0·41	0·05867 ± 0·32	543·3 ± 2·1	545·5 ± 3·5	0·64	554·8 ± 14	2·2
Z3 (*1*;sp,cr)	0·0027	371·6	32·3	1168	4·75	0·2800	0·08825 ± 0·13	0·7135 ± 0·24	0·05863 ± 0·18	545·2 ± 1·3	546·8 ± 2·0	0·68	553·5 ± 7·7	1·6
Z4 (*1*; ± r,c)	0·0064	56·9	4·8	418	4·92	0·1859	0·08776 ± 0·18	0·7107 ± 0·55	0·05874 ± 0·46	542·3 ± 1·9	545·2 ± 4·6	0·61	557·3 ± 20	2·8
Z5 (*1*;o,r,f,c)	0·0058	135·9	11·5	716	6·13	0·1821	0·08797 ± 0·13	0·7105 ± 0·33	0·05858 ± 0·26	543·5 ± 1·4	545·1 ± 2·8	0·62	551·4 ± 12	1·5
Z6 (*1*;lp,fr,cr,i)	0·0062	197·7	17·1	967	6·92	0·2753	0·08691 ± 0·14	0·7008 ± 0·27	0·05848 ± 0·20	537·2 ± 1·5	539·3 ± 2·3	0·67	547·8 ± 9	2·0
Z7 (*3*;lp,cr,i,rs)	0·0140	417·1	36·2	2666	11·8	0·3473	0·08639 ± 0·15	0·6925 ± 0·18	0·05813 ± 0·10	534·1 ± 1·5	534·3 ± 1·5	0·83	538·8 ± 4·5	0·1
Z9 (*5*;f,c,r,o,x)	0·0135	73·5	6·1	768	7·04	0·2033	0·08627 ± 0·17	0·6916 ± 0·41	0·05814 ± 0·34	533·5 ± 1·8	533·7 ± 3·4	0·58	535 ± 15	0·3
HT-99-9; eclogite, Homolka (5542050, 3338763)[9]														
Z1 (*4*;c,p,lp)	0·0231	68·4	4·99	1556	4·79	0·2074	0·07567 ± 0·13	0·5922 ± 0·22	0·0568 ± 0·16	470·2 ± 1·2	472·3 ± 1·7	0·68	482·5 ± 7	2·6
Z2 (*2*;o,c)	0·0575	69·1	5·8	2744	7·79	0·2267	0·08665 ± 0·26	0·6971 ± 0·28	0·05835 ± 0·09	535·7 ± 2·7	537 ± 2·3	0·95	542·8 ± 4	1·4
Z3 (*1*;o,r)	0·0426	103·7	8·8	3649	6·53	0·2481	0·08701 ± 0·18	0·7003 ± 0·20	0·05837 ± 0·08	537·8 ± 1·8	539 ± 1·6	0·92	543·7 ± 3·3	1·1
Z4 (*1*;r,o)	0·0336	81·9	6·1	2543	5·21	0·2061	0·07746 ± 0·23	0·6118 ± 0·25	0·05728 ± 0·10	480·9 ± 2·1	484·7 ± 1·9	0·92	502·4 ± 4·3	4·4
Z5 (*8*;lp,c,cr)	0·0337	42·5	3·2	631	11·2	0·2571	0·07734 ± 0·15	0·6119 ± 0·38	0·05738 ± 0·30	480·2 ± 1·4	484·7 ± 2·9	0·65	506·1 ± 13	5·3
Z6 (*1*;lp,i,cr)	0·0153	39·3	3·1	373	8·56	0·2450	0·08188 ± 0·33	0·6505 ± 0·81	0·05762 ± 0·67	507·3 ± 3·2	508·8 ± 6·5	0·58	515·3 ± 30	1·6
Z7 (*7*;is,c,rs)	0·0288	91·6	7·0	911	14·6	0·1768	0·08027 ± 0·17	0·6376 ± 0·30	0·05761 ± 0·21	497·8 ± 1·6	500·8 ± 2·3	0·70	514·8 ± 9·4	3·4
Z8 (*1*;is,mf)	0·0242	55·1	4·5	453	16	0·2117	0·08474 ± 0·71	0·6766 ± 0·92	0·05791 ± 0·70	524·3 ± 7·1	524·7 ± 7·5	0·65	526 ± 31	0·4
R1B (x,drb)	1·1577	2·81	0·15	71·14	216	0·0294	0·05724 ± 1·53	0·4263 ± 3·35	0·05401 ± 2·59	358·8 ± 10·7	360·5 ± 20·4	0·67	371·5 ± 117	3·5
R2B (x,rb,c)	0·6247	1·95	0·1	70·95	78·8	0·0402	0·05562 ± 1·00	0·4107 ± 2·89	0·05356 ± 2·36	349 ± 6·8	349·4 ± 17·1	0·65	352·4 ± 110	1·0
HT-99-11; eclogite, Louka (5548812, 3342773)[9]														
Z1 (*5*;sp,c,i)	0·0195	89·3	4·94	2005	3·3	0·0061	0·06097 ± 0·19	0·4574 ± 0·24	0·0544 ± 0·14	381·5 ± 1·4	382·4 ± 1·5	0·83	387·8 ± 6·1	1·7
Z2 (*7*;r,mf,c)	0·0175	60·3	3·38	267	16	0·0222	0·06135 ± 0·21	0·4638 ± 0·66	0·05483 ± 0·55	383·8 ± 1·6	386·9 ± 4·2	0·64	405·1 ± 25	5·4
Z3 (*1*;fr?,o)	0·0126	117·5	6·53	539	10·7	0·0117	0·06110 ± 0·21	0·4564 ± 0·43	0·05418 ± 0·33	382·3 ± 1·6	381·8 ± 2·7	0·65	378·3 ± 15	−1·1
Z4 (*1*;o,c,r)	0·0057	82·7	4·61	426	4·45	0·0198	0·06115 ± 0·22	0·4626 ± 0·60	0·05487 ± 0·50	382·6 ± 1·6	386·1 ± 3·8	0·59	407 ± 22·5	6·2
Z5 (*1*;lp,fr,c,i)	0·0027	345·4	28	171·5	30·6	0·3161	0·08166 ± 0·29	0·6340 ± 1·21	0·05631 ± 1·05	506 ± 2·8	498·6 ± 9·6	0·66	464·5 ± 47	−9·3
HT-99-13; amphibolite, Louka (5548745, 3342791)[9]														
Z1 (*1*;fr)	0·0345	89·7	4·94	353	34·7	0·0021	0·06076 ± 0·18	0·4554 ± 0·49	0·05436 ± 0·39	380·2 ± 1·3	381 ± 3·1	0·67	385·9 ± 17	1·5
Z2 (*3*;sp,c)	0·0299	85·5	4·73	1827	5·31	0·0050	0·0609 ± 0·14	0·4568 ± 0·20	0·05438 ± 0·13	381·3 ± 1·0	382 ± 1·3	0·74	386·7 ± 6	1·5
Z3 (*8*;sp,c)	0·0277	67·6	4·46	1358	6·01	0·1487	0·06964 ± 1·04	0·5382 ± 1·06	0·05605 ± 0·15	434 ± 8·8	437·2 ± 7·5	0·99	454·4 ± 6·9	4·6
Z4 (*7*;p,c,cr)	0·0277	53·1	2·96	1102	5·13	0·0135	0·06127 ± 0·14	0·4595 ± 0·26	0·05440 ± 0·19	383·3 ± 1·0	383·9 ± 1·7	0·68	387·6 ± 8·7	1·1
Z5 (*1*;p,i)	0·0038	237·1	20·75	218	24·2	0·3465	0·08721 ± 0·33	0·7043 ± 1·10	0·05858 ± 0·93	539 ± 3·4	541·4 ± 9·2	0·62	551·4 ± 41	2·3
T1B (*10*;x,hb,c)	0·2208	13·3	0·7	215	71·8	0·0114	0·05808 ± 0·81	0·4319 ± 1·11	0·05393 ± 0·67	364 ± 5·7	364·5 ± 6·8	0·80	368 ± 30	1·1

Sample, fraction[1]	Wt.[2] (mg)	U (ppm)	Pb[3] (ppm)	$^{206}Pb/^{204}Pb$[4]	Pb[5] (pg)	Th/U[6]	$^{206}Pb/^{238}U$[7]	$^{207}Pb/^{235}U$[7]	$^{207}Pb/^{206}Pb$[7]	$^{206}Pb/^{238}U$[8] (Ma)	$^{207}Pb/^{235}U$[8] (Ma)	Corr. coeff.	$^{207}Pb/^{206}Pb$[8] (Ma)	Disc.[8] (%)
HT-99-6; orthogneiss, Kyselka Creek valley (5549795, 3341856)[9]														
Z1 (*8*;n,c,rs,i)	0·0165	297·6	21	1265	18·3	0·1094	0·07535 ± 0·21	0·5941 ± 0·28	0·05718 ± 0·16	468·3 ± 1·9	473·5 ± 2·1	0·82	498·5 ± 7	6·3
Z2 (*8*;p,c,i)	0·0172	473·9	33·15	1328	28·7	0·1057	0·07464 ± 0·10	0·5900 ± 0·19	0·05734 ± 0·14	464 ± 0·93	470·9 ± 1·4	0·72	504·5 ± 6	8·3
Z3 (*7*;o,r,c,mf)	0·0130	457·1	34·3	1501	19	0·2412	0·07696 ± 0·23	0·6184 ± 0·27	0·05828 ± 0·14	478 ± 2·1	488·8 ± 2·1	0·86	540·1 ± 6·1	12
Z4 (*1*;lp,fr,cr)	0·0095	529·3	34·7	1159	19·2	0·0648	0·07075 ± 0·17	0·5575 ± 0·26	0·05716 ± 0·17	440·6 ± 1·5	449·9 ± 1·9	0·75	497·7 ± 7·7	12
Z5 (*1*;p,fr,rc)	0·022	182	12·4	7171	2·5	—	0·0712 ± 0·39	0·5911 ± 0·47	0·06021 ± 0·26	443·4	471·5	0·84	611·1 ± 11	
Z6 (*1*;p,fr)	0·017	313·6	22·4	1732	14	—	0·07377 ± 0·21	0·6065 ± 0·41	0·05962 ± 0·34	458·8	481·3	0·55	589·9 ± 15	
Z7 (*9*;lp,c,i)	0·043	72·8	5·5	4075	3·8	—	0·07881 ± 0·18	0·6402 ± 0·34	0·05891 ± 0·28	489·1	502·4	0·54	563·9 ± 12	
Z8 (*1*;lp)	0·010	268·3	16·9	787	13	—	0·06150 ± 0·49	0·5361 ± 0·86	0·06322 ± 0·68	384·7	435·9	0·61	715·7 ± 29	
M2 (e,y,i)	0·0016	11587	2270	5693	12·2	8·507	0·06067 ± 0·33	0·4530 ± 0·34	0·05416 ± 0·10	379·7 ± 2·5	379·4 ± 2·2	0·99	377·7 ± 2·4	−0·5
M4 (e,c,y,i)	0·0016	5123	1256	1424	21·8	11·53	0·06049 ± 0·13	0·4509 ± 0·24	0·05406 ± 0·18	378·6 ± 1·0	377·9 ± 1·5	0·67	373·5 ± 8·2	−1·4
HT-99-1; felsic remobilizate, Tisova (5548745, 3342791)[9]														
T1 (x,db)	0·1999	110·4	5·9	553	149	0·0292	0·05850 ± 1·42	0·4333 ± 2·19	0·05372 ± 0·94	366·5 ± 10·1	365·5 ± 13·4	0·95	359·4 ± 43	−2·0
T2 (yb,c)	0·1120	96·8	5·4	304	142	0·0597	0·06061 ± 0·22	0·4496 ± 0·66	0·05379 ± 0·53	379·4 ± 1·6	377 ± 4·1	0·67	362·3 ± 24	−4·8

[1]Z, zircon, abraded for 2·5—8 h, using technique of Krogh (1982); M, monazite; T, titanite; R, rutile. Italic number is number of grains in fraction; titanite and rutile are multigrain fractions. c, clear; cr, ± cracks; db, dark brown; drb, dark red—brown; e, euhedral; f, flat; fr, fragment; hb, honey brown; i, ± inclusions; is, isometric; lp, long-prismatic; mf, multifaceted; n, needles; o, oval; p, prismatic; r, round; rb, red—brown; rc, ± recrystallized; rs, resorbed; sp, short-prismatic; y, yellowish; yb, yellow—brown; x, xenomorphic;
[2]Maximum errors are ±50% for weights <0·002 mg, and ±20% for weights >0·002 mg.
[3]Radiogenic Pb.
[4]Measured ratio, corrected for spike and Pb fractionation.
[5]Total common Pb in analyses corrected for fractionation and spike.
[6]Model ratio calculated from $^{208}Pb/^{206}Pb$ ratio.
[7]Common Pb correction for blank Pb and U, and Stacey & Kramers (1975) model Pb composition equivalent to the interpreted age of the individual grains. Errors are 1 standard error of the mean in percent for ratios.
[8]Corrected for blank and common Pb; errors are 2 standard errors of the mean when expressed in Ma.
[9]Gauss Krüger coordinates.

time, thus reflecting major recrystallization at *c.* 380 Ma in this rock. The same *c.* 380 Ma event also affected 'gabbro' HT-99-9, as evidenced by the lower intercept age of 377 Ma. It is here manifested in resorption and new zircon growth at the crystal rims, discordance of the 540 Ma zircons, strongly overprinted high-pressure assemblages by granulite-facies mineral assemblages at high temperatures above 750°C (see kyanite breakdown products), and distinct decompression textures that indicate hydration during exhumation and associated decompression melting in a granulite-facies to upper amphibolite-facies environment. Furthermore, the rutile ages indicate cooling to *c.* 450–400°C (e.g. Mezger *et al.*, 1989).

Based on mineral compositions and textures, the protolith of high-pressure granulite HT-99-4a was a coarse-grained porphyritic gabbrodiorite with phenocrysts of Ca-plagioclase in a more mafic matrix. The textures also indicate equilibration under high-pressure and high-temperature conditions (Table 1; Štědrá, 2001) at depths greater than 50 km, which correspond to the lower levels of thickened continental crust. Coexistence of omphacite and spinel reflects disequilibrium between the light-coloured, Al-rich domains and the darker matrix. The limited element mobility between the Al-rich (former Ca-plagioclase) and matrix domains, also reflected by differing garnet compositions and zoning patterns, may be explained by dry conditions prevailing at this lower-crustal level. HT-99-4a also has a distinct isotope and trace element composition compared with the eclogites. Its trace element composition, with high Sr/Y, Zr/Sm, Nd/Sm and Al contents, has affinities to adakites, which were originally proposed to be the products of melting of young, and thus still hot, subducted oceanic crust (e.g. Defant & Drummond, 1993). Compatible element contents, such as Mg, Cr, Ni, and Mg number, however, are lower than those of typical adakites. The array of concordant zircon ages from *c.* 545 Ma to 535 Ma indicates that protolith crystallization started in late Cadomian times at *c.* 545 Ma and, considering the internal zircon structures described above, occurred in several stages. The timing of final resorption and subsequent crystallization of new zircon (bright luminescent zircon rim in Fig. 2e) was not determined, because these rims were (1) removed by abrasion and (2) probably U-poor, as deduced from the brightness of the CL picture. Any rim material that remained after abrasion would have therefore contributed little radiogenic lead with only a minor resultant effect on the bulk analyses. We assume, however, that this sample stayed at high pressures and high temperatures until Variscan exhumation at *c.* 380 Ma. At this time, decompression was associated with partial melting of the MLC rock pile, including the high-pressure rocks, as evidenced, for example, by leucosome HT-99-1. The latter, however, is spatially associated with HT-99-9-type eclogites, and has, as yet, not been observed in association with high-pressure-type granulites such as HT-99-4a.

The LILE contents and isotopic composition of samples HT-99-7 andHT-99-8, both part of the metagabbro suite in the MLC–TBU boundary zone, indicate a different protolith compared with the eclogites. The trace-element patterns reveal some similarities to the geochemistry of E-MORB and calc-alkaline volcanics from the Andes (Fig. 8b; Hickey *et al.*, 1986), although the latter generally have lower HFSE and higher Sr contents. The composition of the metagabbros could also be associated with a rift-related setting, as suggested by Štědrá *et al.* (2002). New data of Timmermann *et al.* (in preparation) indicate an emplacement age for the metagabbros of around 500 Ma, and confirm an upper intercept age of 496 ± 1 Ma from a gabbro pegmatite (Bowes & Aftalion, 1991). The metagabbros are thus about 40–50 Myr younger than the protoliths of the MLC eclogites. The geochronological data validate field relationships, such as amphibolite inclusions within the metagabbros, intrusion relationships with the 513 +7/–6 Ma Teplá orthogneiss (Dörr *et al.*, 1998), and ambiguous mutual relationships of metagabbros and orthogneisses (Kachlík, 1997*b*; Tonika, 1998) that suggest a younger age for the metagabbros than for the MLC host rock. The intrusive relationships of the metagabbros with the host rocks of both the MLC and the structurally overlying Teplá crystalline unit (TCU), and the evidence of *c.* 500 Ma monazite growth in the paragneisses of the TCU in response to gabbro emplacement (Timmermann *et al.*, in preparation), imply that both units must have been associated already at that time. Mineral assemblages and compositions reflect a metamorphic overprint onto the primary magmatic assemblage at high temperatures and pressures; however, these metagabbros did not experience true eclogite-facies conditions (Štědrá *et al.*, 2002). This strongly suggests a pre-500 Ma minimum age for eclogite-facies metamorphism.

Field relationships and petrography (e.g. Fig. 5a) suggest that amphibolite HT-99-13 represents the retrogressed equivalent of associated eclogite HT-99-11. Its trace element pattern, however, is distinct, and the Nd–Sr isotopic composition is less primitive, similar to that of high-pressure granulite HT-99-4a and a garnet amphibolite reported by Beard *et al.* (1995). The selective depletion of certain elements, such as Rb, Sr, Sm and Nd, relative to other incompatible elements (Fig. 8) and to eclogite HT-99-11, points to element mobility and alteration of its isotope composition as a result of a secondary process. Differences between the REE and Nd isotope compositions of the two rocks, however, cannot as readily be attributed to post-crystallization disturbance, given that other lithologies examined in this study do not appear to have undergone significant modification during

Table 5a: Previous geochronological data from the Mariánské Lázně Complex

Locality	Age	Rock type	Isotopes/mineral	Interpretation	Reference
U–Pb					
3 km S of Becov	854 ± 130 Ma (UI)	feldspar gneiss	zircon	protolith age	Bowes & Aftalion (1991)
Výškovice	496 ± 1 Ma	Grt-metagabbro	zircon	gabbro crystallization	Bowes & Aftalion (1991)
Sm–Nd					
Mnichov	409 ± 8 Ma (420 Ma)	eclogite (group II)	Grt–Omp cores	pre-eclogite amph.-facies metamorphism?	Beard *et al.* (1995)
Louka	377 ± 7 Ma	eclogite (group I)	Grt–Omp	eclogite formation (?)	Beard *et al.* (1995)
Mnichov	367 ± 4 Ma	eclogite (group II)	Grt–Omp rims	eclogite formation?	Beard *et al.* (1995)
$^{40}Ar/^{39}Ar/K–Ar$					
Výškovice	397 ± 5 Ma	metagabbro	K–Ar/Hbl	normal fault at SW margin MLC	Zulauf (1997*b*)
Výškovice	385 ± 8 Ma; 386 ± 5 Ma	metagabbro	K–Ar/Hbl	NW-directed thrusting	Zulauf (1997*b*)
NW of Tisová	379 ± 4 Ma; 380 ± 4 Ma	post-tect. pegmatite	$^{40}Ar/^{39}Ar$ /Hbl	cooling	Bowes *et al.* (2002)
N of Poutnov	380–370 Ma		K–Ar/Hbl		Kreuzer *et al.* (1992)
W of Hanov	375 Ma		K–Ar/Hbl		Zulauf (1997*b*)
Becov	372 Ma	Grt-metagabbro	$^{40}Ar/^{39}Ar$/Hbl	cooling	Dallmeyer & Urban (1994)
Central MLC	371 Ma		$^{40}Ar/^{39}Ar$/Hbl		Zulauf (1997*b*)
Kladska unit	386 Ma	metabasalt	K–Ar/Hbl	cooling	Kreuzer *et al.* (1989)
MLC	366 ± 1 Ma	white mica			Zulauf (1997*b*)
Výškovice	369 Ma	amphibolite	Bt		Kreuzer *et al.* (1992)
Kladska unit	359 Ma	metabasalt	K–Ar/Bt	cooling	Kreuzer *et al.* (1989)
Výškovice	317 ± 4 Ma	metagabbro	K–Ar/Bt	in normal fault	Zulauf (1997*b*)

UI, upper intercept; LI, lower intercept.

metamorphism. What is clear is that although the two rocks may not be geochemically related, the geochronological data and internal zircon structures in both rocks indicate that their protoliths are of similar age, and that both rocks shared a similar post-peak metamorphic evolution. The protolith age of HT-99-13 is *c.* 540 Ma, coeval with the crystallization age for zircon from high-pressure granulite HT-99-4a and eclogite HT-99-9. Similar to the older zircon in the associated eclogite HT-99-11, Z5 of the amphibolite has a distinctly higher U content compared with the other, younger fractions. The 540 Ma component is still present as inheritance within some of the zircon cores (e.g. Fig. 5d). Other similarities between the zircon grains of associated samples HT-99-11and HT-99-13 are the internal 'fir-tree' zoning structures and the concordant zircon ages around 384 ± 2 Ma. As in eclogite HT-99-11, the *c.* 380 Ma event is interpreted to have caused the formation of the main internal zircon structures under conditions of upper amphibolite facies to granulite facies in the presence of a partial melt, a scenario typical for Variscan exhumation and associated decompression melting. The titanite age of 365 ± 7 Ma is taken to reflect the timing of the retrograde amphibolite-facies metamorphism, at temperatures of 650–600°C (e.g. Heaman & Parrish, 1991; Zhang & Schärer, 1996).

Variably discordant U–Pb analyses from felsic orthogneiss HT-99-6 reflect complex inheritance and recrystallization patterns. Therefore, no major conclusion can be drawn with respect to the age of orthogneiss crystallization or to the degree of Variscan overprinting. We can, however, assume that zircon xenocrysts were derived from several sources of Cadomian and/or pre-Cadomian age (e.g. Table 5a). In contrast, concordant monazite ages of 380 ± 3 Ma are coeval with the concordant *c.* 380 Ma zircon ages of samples HT-99-11 and HT-99-13, and the lower intercept age (377 ± 27 Ma) of eclogite HT-99-9, indicating that all of these rocks experienced the same tectonometamorphic event at this time. As the orthogneisses show no evidence of a high-pressure history, and may have been tectonically emplaced into the mafic to intermediate host rocks of the MLC, the consistency of the *c.* 380 Ma ages in the various rock types of the MLC indicates that (1) all of the rock units of the MLC associated at present were assembled at that time, and (2) the *c.* 380 Ma Variscan event, which was

Table 5b: Available geochronological data from the Teplá Barrandian Unit

Locality	Age	Rock type	Isotopes/mineral	Interpretation	Reference
U–Pb					
Dobříš	585 ± 7, 568 ± 3 Ma (LI)	rhyolite boulders	zircon	subduction-related volcanism	Dörr *et al*. (2002)
Neukirchen–Kdyne	524 ± 3 Ma–522 ± 2 Ma	(grano)diorites	zircon	intrusions in transtensive shear zones	Dörr *et al*. (2002)
N of Domažlice	551 ± 19 Ma	paragneiss	Th(U)–Pb/EMS/Mnz	LP/HT metamorphism	Zulauf *et al*. (1999)
Domažlice/Havlovice	542 ± 23 Ma	paragneiss	Th(U)–Pb/EMS/Mnz	LP/HT metamorphism	Zulauf *et al*. (1999)
Předni Skalá	540 ± 16 Ma	paragneiss	Th(U)–Pb/EMS/Mnz	LP/HT metamorphism	Zulauf *et al*. (1999)
Teplá	513 +7/–6 Ma (UI)	Tepla orthogneiss	zircon	protolith age	Dörr *et al*. (1998)
Lestkov	511 ± 10 Ma	Lestkov orthogneiss	zircon	protolith age	Dörr *et al*. (1998)
Hanov	516 ± 10 Ma	Hanov orthogneiss	zircon	protolith age	Dörr *et al*. (1998)
ZTD (Teplá–Domažlice)	~480 Ma	metapegmatites	zircon, monazite	pegmatite emplacement and crystallization	Glodny *et al*. (1998)
Neukirchen–Kdyne	359 ± 2/361 ± 4 Ma (UI)	Teufelsberg diorite	zircon	emplacement	Bues *et al*. (2002)
Rb–Sr					
Teplá cryst. complex	487 ± 5 Ma–475 ± 5 Ma	metapegmatites	Rb–Sr/Ms	pegmatite emplacement and crystallization	Glodny *et al*. (1998)
Domažlice CC	494 ± 6 Ma–484 ± 5 Ma	metapegmatites	Rb–Sr/	pegmatite emplacement and crystallization	Glodny *et al*. (1998)
Teplá cryst. complex	375–372 ± 4 Ma	metapegmatites	Rb–Sr/recryst. Ms	end of deformational activity	Glodny *et al*. (1998)
Domažlice CC	376–372 ± 4 Ma	pegmatite	Rb–Sr/recryst. Ms/Kfs	end of deformational activity	Glodny *et al*. (1998)
$^{40}Ar/^{39}Ar/K–Ar$					
Neukirchen–Kdyne	549–547 ± 7 Ma	Smržovice diorite	K–Ar/Hbl	excess argon?	Bues *et al*. (2002)
Neukirchen–Kdyne	495 ± 6 Ma	Smržovice diorite	K–Ar/Bt	minimum cooling age	Bues *et al*. (2002)
	383 Ma	amphibolite	Hbl	post-metamorphic cooling	Dallmeyer & Urban (1994)
	375–362 Ma	schist/gneiss	Ms	cooling	Dallmeyer & Urban (1994)
Teplá cryst. complex	369–366 Ma		K–Ar/^{40}Ar/^{39}Ar /Ms	in staurolite isograde	Zulauf (1997*b*)
Teplá cryst. complex	351 ± 8 Ma	phyllite	K–Ar/sericite	chlorite–sericite zone	Zulauf (1997*b*)
Neukirchen–Kdyne	342 ± 4 Ma	Teufelsberg diorite	K–Ar/Bt	minimum cooling age	Bues *et al*. (2002)
Teplá	316 ± 7 Ma	paragneiss	K–Ar/sericite		Zulauf (1997*b*)
Teplá	371–362 Ma		K–Ar/Bt		Zulauf (1997*b*)

UI, upper intercept; LI, lower intercept.

accompanied by decompressional partial melting, was not the peak, high-pressure event.

Decompression melting in the host rocks of the MLC during Variscan exhumation is evidenced also by the presence of newly formed melts that crystallized in structurally weak zones. An example of this is sample HT-99-1, a felsic leucosome in the neck of a mafic boudin (Fig. 7a). The isotope composition of the leucosome is similar to that of high-pressure granulite HT-99-4a and the amphibolites. This supports our field observations that this felsic partial melt was extracted from the intermediate to mafic host rock of the MLC. Titanite that formed during crystallization of the anatectic melt gives an age of 378 ± 4 Ma, which we take as the minimum estimate for the age for high-temperature metamorphism and anatexis of the amphibolites in the MLC. This interpretation agrees with zircon growth in the mafic eclogite HT-99-11 in an upper amphibolite-facies to granulite-facies environment, and with monazite formation in orthogneiss HT-99-6. This sample thus provides unequivocal

Table 5c: Available geochronological data from the Erbendorf–Vohenstrauss Zone

Locality	Age	Rock type	Isotopes/mineral	Interpretation	Reference
U–Pb					
KTB profile	496–476 Ma (UI)	metagabbro (± ophitic)	zircon	protolith crystallization	von Quadt (1997)
KTB pilot borehole	481–476 Ma	eclogite	zircon (core/whole)	magmatic	Grauert *et al.* (1994)
	487 ± 13 Ma	paragneiss	SHRIMP/zircon	overgrowth	Söllner & Nelson (1995)
Wendersreuth	~480 Ma	metapegmatites	zircon, monazite	pegmatite emplacement and crystallization	Glodny *et al.* (1998)
S ZEV	457 ± 2 Ma (LI)	augengneiss	zircon	protolith crystallization	Teufel (1988)
	457 Ma	orthogneiss	monazite	resetting at 380 Ma? (discordant?)	Teufel *et al.* (1992)
KTB pilot borehole	405 Ma (LI)	leucocratic orthogneiss	zircon	intrusion of orthogneiss protolith	Grauert *et al.* (1994)
Ödenthal, S ZEV	404 ± 30 Ma (UI)	orthogneiss	zircon	maximum intrusion age	Teufel (1988)
	381 Ma	paragneiss	SHRIMP/zircon	overgrowth	Söllner & Nelson (1995)
	380 ± 3 Ma, 378 ± 3 Ma	paragneiss	monazite	metamorphism	Teufel (1988)
Rb–Sr					
Reuth–Erbendorf	545 ± 16 Ma	granodiorite	Rb–Sr/WR-isochron	inheritance	Holl *et al.* (1989)
	530–525 Ma		Rb–Sr/WR	igneous event	Teufel (1988)
	481 ± 5–473 ± 5 Ma	metapegmatites	Rb–Sr/Ms	post-emplacement cooling ages	Glodny *et al.* (1998)
Ödenthal, S ZEV	379 ± 15 Ma	orthogneiss	Rb–Sr/WR-isochron		Teufel (1988)
	376 ± 4–371 ± 4 Ma	metapegmatites	Rb–Sr/recryst. Ms	end of deformational activity	Glodny *et al.* (1998)
K–Ar					
western ZEV	401–391 Ma	amphibolite	K–Ar/Hbl	inherited/excess argon	Kreuzer *et al.* (1989)
western ZEV	378 ± 2 Ma	amphibolite	K–Ar/Hbl	early Devonian regional metamorphism	Kreuzer *et al.* (1989)
western ZEV	385–384 Ma	gneiss	K–Ar/Bt	early Devonian regional metamorphism	Kreuzer *et al.* (1989)
ZEV/EGZ	377 ± 3–371 ± 3 Ma	gneisses and pegmatoids	K–Ar/Ms	end of Devonian regional MP metamorphism	Ahrendt *et al.* (1997)
western ZEV	373–366 Ma	gneiss	K–Ar/Ms	end of regional metamorphism	Kreuzer *et al.* (1989)
eastern ZEV	330–303 Ma		K–Ar/Hbl		Kreuzer *et al.* (1989)

UI, upper intercept; LI, lower intercept; SHRIMP, sensitive high-resolution ion microprobe; WR, whole rock.

evidence that the *c.* 380 Ma zircon ages from the eclogites date the decompression melting that accompanied exhumation through the granulite stability field, and not the time of eclogitization as suggested by Beard *et al.* (1995). A titanite age of 366 Ma coincides with titanite growth in sample HT-99-13 and with resetting of rutile in eclogite HT-99-9. The 366 Ma age also probably represents resetting during cooling, as it overlaps with $^{40}Ar/^{39}Ar$ and K–Ar cooling ages of biotite and hornblende (Table 5a) in the MLC.

Implications for the tectonic evolution of the MLC and related units

One of the most significant findings of our multidisciplinary study is that, although the rocks of the MLC vary in mineral composition and geochemistry, they fall into two age groups (*c.* 540 Ma, *c.* 380 Ma) that do not correspond to the previous model for the MLC involving early Ordovician rifting and associated ocean-floor formation (Bowes & Aftalion, 1991; Jelínek *et al.*, 1997; Floyd *et al.*, 2000). Instead, our U–Pb data show that eclogite,

Table 5d: Available geochronological data from the Münchberg Massif

Locality	Age	Rock type	Isotopes/mineral	Interpretation	Reference
U–Pb					
Steinach	609+17/−19 Ma (UI)	rhyolite	zircon	volcanic activity	Dörr *et al*. (2002)
Weissenstein area	525+40/−31 Ma (UI)	eclogite and metagabbro	zircon	protolith age of basaltic lava/tuff	Gebauer & Grünenfelder (1979)
Weissenstein area	380+14/−22 Ma (LI)	eclogite and metagabbro	zircon	eclogite-facies metamorphism?	Gebauer & Grünenfelder (1979)
Lu–Hf/Sm–Nd/Rb–Sr					
Oberkotzau (NE MM)	405 ± 7 Ma, 384 ± Ma	light eclogite	Lu–Hf/Grt-Omp	garnet growth during eclogite formation	Scherer *et al*. (2002)
Weissenstein (SW MM)	397 ± Ma, 398 ± Ma	dark eclogite	Lu–Hf/Grt-Omp	garnet growth during eclogite formation	Scherer *et al*. (2002)
Weissenstein (SW MM)	480 ± 23 Ma	eclogite	Sm–Nd/WR	igneous formation of eclogite protolith	Stosch & Lugmair (1990)
Weissenstein (SW MM)	395–380 Ma	eclogite	Sm–Nd; Rb–Sr	eclogite metamorphism	Stosch & Lugmair (1990)
Weissenstein area	379 ± 12 Ma	eclogite	Rb–Sr/Hbl, phengite	post-eclogite	Gebauer & Grünenfelder (1979)
K–Ar					
Hangendserie	379 ± 3 Ma, 372 ± 3 Ma	amphibolite/ hbl-gneiss	K–Ar/Hbl	(end of) MP amphibolite-facies metamorphism	Kreuzer *et al*. (1989)
Hangendserie	388 ± 2/382–379 ± 3 Ma	eclogite	K–Ar/Ms (coarse/fine)		Kreuzer *et al*. (1989)
Liegendserie	381 ± 1 Ma	gneiss	K–Ar/Hbl, Ms		Kreuzer *et al*. (1989)
Randamphibolit	401 ± 4 Ma, 384 ± 3 Ma	amphibolite	K–Ar/Hbl		Kreuzer *et al*. (1989)
Prasinit–Phyllit-Serie	366 ± 2 Ma	phyllite	K–Ar/Ms	late Devonian thermal or tectonic overprint	Kreuzer *et al*. (1989)

UI, upper intercept; LI, lower intercept; WR, whole rock.

high-pressure granulite, and amphibolite protoliths from the MLC are of late Cadomian age (*c*. 540 Ma). The rocks are younger than the episodes of Cadomian igneous activity in the Avalonian–Cadomian terranes, the last of which is represented in the adjacent TBU by felsic volcanism ranging from *c*. 590 to 565 Ma in age (e.g. Dörr *et al*., 2002).

The geochemical signatures of the mafic eclogites of the MLC are compatible with the generation of their protoliths as normal to slightly enriched ocean-floor basalts. In contrast, the high-pressure granulite HT-99-4a has a different origin, geochemically forming a distinct group with the leucosome and amphibolite samples. In some respects similar to adakites, the trace element composition of HT-99-4a, considering that it is unlikely to be the effect of crystal fractionation, could be explained by partial melting of either (1) subducted young oceanic crust, or (2) the lowest part of thickened (>50 km) continental crust. In case (1) the slab-derived partial melts would intrude parts of the lower levels of the thickened crust of the overlying TBU (≥50 km thick), where they equilibrated statically at high pressures and temperatures. Case (2) requires the underplating of basaltic magma in order to reach the very high temperatures required to melt basic granulites in the lower crust (e.g. Defant *et al*., 2002, and references therein). The second scenario is consistent with the tectonic model for the TBU and the adjacent MLC proposed by Zulauf *et al*. (1999). Those workers envisaged lithospheric delamination caused by slab breakoff after arc/microterrane subduction under the northern Gondwana margin (i.e. the present TBU), and resulting upwelling of asthenosphere in the late Cadomian, at *c*. 540 Ma. To achieve the current distribution of rocks in the MLC, subduction of the late Cadomian ocean floor beneath the Teplá–Barrandian plate is necessary to juxtapose the current eclogites with the lowest crust of the TBU (high-pressure granulite). At the same time, *c*. 550–540 Ma (Zulauf *et al*., 1999), crustal thickening and medium- to low-grade metamorphism at mid- to upper-crustal levels happened in the overlying

TBU. Within the related allochthonous nappes of the Münchberg Massif and the Erbendorf–Vohenstrauss Zone, however, late Cadomian ages are rare or absent (Table 5c and d). A magmatic event similar to that of the MLC is indicated in the Erbendorf–Vohenstrauss Zone by 530–525 Ma Rb–Sr whole-rock isochrons from amphibolite and interlayered orthogneiss (Teufel, 1988), and by 545 Ma Rb–Sr whole-rock ages from granodiorites (Holl *et al.*, 1989).

The only rock types in the MLC coeval with the widely proposed Cambro-Ordovician intracontinental rifting event that led to the break-up of Gondwana are the *c.* 500 Ma metagabbros in the MLC–TBU boundary zone (Bowes & Aftalion, 1991; Timmermann *et al.*, in preparation). The fact that their emplacement caused monazite growth in paragneisses of the structurally overlying TBU (Timmermann *et al.*, in preparation) requires that assembly of the MLC with the mid-crustal level of the currently exposed TBU had been accomplished at that time. Metagabbro intrusion has also been dated in the Erbendorf–Vohenstrauss Zone from 496 to 476 Ma (von Quadt, 1997). These, and the slightly younger U–Pb zircon ages of the eclogites (481–476 Ma; Grauert *et al.*, 1994), zircon overgrowth in paragneisses (487 ± 13 Ma; Söllner & Nelson, 1995), and pegmatite emplacement (481–473 ± 5 Ma; Glodny *et al.*, 1998) support the occurrence of an igneous event within this interval (Table 5c). For the Münchberg Massif, replotting of U–Pb analyses from eclogite and metagabbro (Gebauer & Grünenfelder, 1979; Ludwig, 2001) yields concordant zircon ages of 496 ± 3 Ma for metagabbro crystallization, corresponding precisely to the age of the MLC and Erbendorf–Vohenstrauss Zone metagabbros.

Zircon growth at *c.* 380 Ma reflects the end of ocean closure in the Variscan and final collision of the TBU with the Saxothuringian unit in this area (e.g. Matte *et al.*, 1990). Previously reported, slightly younger Sm–Nd isochron ages of 377 ± 7 Ma and 367 ± 4 Ma from eclogites of the MLC were proposed to date the timing of subduction of the Saxothuringian ocean below the TBU (Beard *et al.*, 1995). However, we have shown with our study that zircon ages around 380 Ma date exhumation of rocks that were juxtaposed at depth (eclogites, high-pressure granulite), along with associated decompression melting of eclogites under upper amphibolite- to granulite-facies conditions. Zircon growth after the pressure peak during uplift along an isothermal decompression P–T path has been recognized recently by several workers (e.g. Roberts & Finger, 1997; Fernandez-Suarez *et al.*, 2002; Whitehouse & Platt, 2003). In the southern Bohemian Massif, Roberts & Finger (1997) explained this feature by zircon saturation in a partial melt coexisting with the restite granulite. Although not dating eclogitization, the 377–367 Ma Sm–Nd isochron ages of Beard *et al.* (1995) agree well with our new titanite and rutile ages from the MLC, which we take to date crystallization of such partial melts and resetting during cooling. Isotopic re-equilibration of Sm–Nd isotope systematics is not uncommon in high-pressure rocks, especially during deformation-enhanced fluid circulation in the course of retrograde amphibolite-facies metamorphism (e.g. Ganguly *et al.*, 1998; Luais *et al.*, 2001), and is invoked here to explain the Sm–Nd isochron ages of Beard *et al.* (1995). An Ar–Ar hornblende age of 379 Ma from a post-metamorphic, cross-cutting pegmatite in the MLC (Bowes *et al.*, 2002) further supports our interpretation that *c.* 380 Ma ages do not correspond to the high-pressure metamorphism but instead to exhumation. Other K–Ar and Ar–Ar ages for hornblendes (T_c *c.* 500°C; e.g. Cliff, 1993) in the MLC rocks give a range from 397 to 370 Ma (Table 5a), partly overlapping with the zircon and monazite ages from this study. This age cluster, the 'fir-tree' sector zoning in 380 Ma zircon, and the K–Ar and Ar–Ar ages for mica (T_c *c.* 300°C; e.g. Cliff, 1993) from 370 to 360 Ma (Table 5a), provide evidence for (very) fast exhumation and cooling of the MLC rocks at that time. Similarly, the Variscan regional high-grade metamorphism around 380 Ma and subsequent rapid exhumation is documented in the Erbendorf–Vohenstrauss Zone and Münchberg Massif (Table 5c and d).

We have shown with our study, however, that the age for high-pressure metamorphism in this area can not be constrained by U–Pb zircon geochronology. A possible timing of eclogite formation in the MLC could have been just before the *c.* 380 Ma granulite-facies exhumation stage, as proposed by Zulauf (1997*b*) on the basis of thermal modelling. This would be coeval with high-pressure metamorphism in the Münchberg Massif, dated recently by Lu–Hf geochronology at ≤405 Ma (Scherer *et al.*, 2002; Table 5d). In comparison, Sm–Nd and Rb–Sr isochrons for Münchberg Massif eclogites gave slightly younger ages of 395–380 Ma, but were also interpreted as the eclogitization phase (Stosch & Lugmair, 1990). The 395–380 Ma isochron ages, however, may have been reset during later regional metamorphism, probably under the influence of fluids (Miller *et al.*, 2002). As discussed above, the same re-equilibration of the Sm–Nd isotope system had taken place in the eclogites of the MLC during later regional metamorphism. However, a Sm–Nd isochron age of 409 ± 8 Ma derived from a garnet core, omphacite, and bulk-rock analyses of an eclogite of the MLC, although interpreted to reflect prograde metamorphism (Beard *et al.*, 1995), overlaps within error with the Lu–Hf ages for the Münchberg Massif of Scherer *et al.* (2002). An even earlier, late Cadomian to early Cambrian eclogitization is suggested instead by the absence of high-pressure assemblages within the *c.* 500 Ma metagabbro intrusions from the MLC (Bowes & Aftalion, 1991). Alternatively, the high-pressure rocks may have been tectonically emplaced into

the MLC host rocks during Variscan exhumation from deep levels to a position adjacent to the metagabbros. Therefore, we conclude that conventional zircon geochronology, as reported here, cannot unambiguously constrain the age of the high-pressure metamorphism in this area. To do that, other methods must be employed. These could be *in situ* techniques, such as sensitive high-resolution ion microprobe (SHRIMP) or laser ablation multicollector inductively coupled plasma–mass spectrometry (ICP-MS), using zircon inclusions within high-pressure garnets to yield a minimum age for the high-pressure event. Alternatively, the relatively new method of Lu–Hf isochron dating by multicollector ICP-MS could be employed on garnet-bearing high-pressure rocks rich in REE. When taking care to avoid Hf-rich inclusions in garnet, this method can be successfully employed to date high-pressure metamorphism in a more precise and less spurious way compared with Sm–Nd isochron dating (e.g. Duchêne *et al.*, 1997; Scherer *et al.*, 2002).

ACKNOWLEDGEMENTS

We thank V. Kachlik for fruitful discussions in the field, M. Spallek for field assistance, and H. Billin, R. Branson, K. David, U. Glenz, M. Grünhäuser, J. Schastok and I.Vavrín for assistance in the various laboratories and analytical facilities. S. Wulf is thanked for carrying out the CL imaging at the GFZ in Potsdam. We appreciate the valuable comments of P. D. Kempton, F. Finger, P. O'Brien, D. Rubatto and J. Hanchar for improving this paper. This research was supported by the Palaeozoic Amalgamation of Central Europe (PACE) research network (CORDIS TMR contract number ERBFMRX-CT970136). This paper is NIGL publication 588.

REFERENCES

Ahrendt, H., Glodny, J., Henjes-Kunst, F., Höhndorf, A., Kreuzer, H., Küstner, W., Müller-Sigmund, H., Schüssler, U., Seidel, E. & Wemmer, K. (1997). Rb–Sr and K–Ar mineral data of the KTB and the surrounding area and their bearing on the tectonothermal evolution of the metamorphic basement rocks. *Geologische Rundschau* **86**(Supplement), S251–S257.

Anczkiewicz, R., Thirlwall, M. & Platt, J. (2002). Influence of inclusions and leaching techniques on Sm–Nd and Lu–Hf garnet chronology. *Geochimica et Cosmochimica Acta* **66**(Supplement 1), A19.

Beard, B. L., Medaris, L. G., Johnson, C. M., Jelínek, E., Tonika, J. & Riciputi, L. R. (1995). Geochronology and geochemistry of eclogites from the Mariánské Lázně Complex, Czech Republic: implications for Variscan orogenesis. *Geologische Rundschau* **84**, 552–567.

Blundy, T. & Holland, J. (1994). Non-ideal interaction in calcic amphiboles and their bearing on amphibole–plagioclase thermometry. *Contributions to Mineralogy and Petrology* **116**, 433–447.

Bowes, D. R. & Aftalion, M. (1991). U–Pb zircon isotope evidence of Early Ordovician and Late Proterozoic units in the Mariánské Lázně Complex, Central European Hercynides. *Neues Jahrbuch für Mineralogie, Monatshefte* **7**, 315–326.

Bowes, D. R., van Breemen, O., Hopgood, A. M. & Jelínek, E. (2002). $^{40}Ar/^{39}Ar$ isotopic evidence for mid-Devonian post-metamorphic pegmatite emplacement in the Mariánské Lázně Complex, Bohemian Massif, Central European Hercynides. *Neues Jarbuch für Mineralogie, Monatshefte*, **10**, 445–457.

Brueckner, H. K., Medaris, L. G. & Bakun-Czubarow, N. (1991). Nd and Sr age and isotope patterns from Variscan eclogites of the eastern Bohemian Massif. *Neues Jahrbuch für Mineralogie, Abhandlungen* **163**, 169–196.

Bues, C., Dörr, W., Fiala, J., Vejnar, Z. & Zulauf, G. (2002). Emplacement depth and radiometric ages of Paleozoic plutons of the Neukirchen–Kdyně massif: differential uplift and exhumation of Cadomian basement due to Carboniferous orogenic collapse (Bohemian Massif). *Tectonophysics* **352**, 225–243.

Burton, C. W. O. & O'Nions, R. K. (1991). High-resolution garnet chronometry and the rates of metamorphic processes. *Earth and Planetary Science Letters* **107**, 649–671.

Burton, K. W., Cohen, A. S., Kohn, M. J. & O'Nions, R. K. (1995). The relative diffusion of Pb, Nd, Sr, and O in garnet. *Earth and Planetary Science Letters* **133**, 199–211.

Carswell, D. A. (1990). Eclogites and the eclogite facies: definitions and classification. In: Carswell, D. A. (ed.) *Eclogite Facies Rocks*. New York: Chapman & Hall, pp. 1–13.

Cháb, J. (1973). Fosilní oceánická kůra a svrchní plášť' na dnešním povrchu souší. *Věstník Ústředního ústavu geologického* **48**, 303–310.

Cháb, J., Šrámek, J., Pokorný, L., Chlupáčová, M., Manová, M., Vejnar, Z., Waldhauserová, J. & Žáček, V. (1997). The Teplá–Barrandian Unit. In: Vrana, S. & Štědrá, V. (eds) *Geological Model of Western Bohemia Related to the KTB Borehole in Germany*. *Journal of Geological Sciences, CGS Prague* **47**, 80–104.

Cliff, R. A. (1993). Isotopic dating of metamorphism and cooling. *School Earth and Planetary Science* **7**, 131–140.

Dallmeyer, R. D. & Urban, M. (1994). Variscan vs. Cadomian tectonothermal evolution within the Teplá–Barrandian zone, Bohemian Massif, Czech Republic: $^{40}Ar/^{39}Ar$ mineral and whole-rock slate/phyllite ages. *Journal of the Czech Geological Society* **39**, 21–22.

Davidson, A. & van Breemen, O. (1988). Baddeleyite–zircon relationships in coronitic metagabbro, Grenville Province: implications for geochronology. *Contributions to Mineralogy and Petrology* **100**, 291–299.

Defant, M. J. & Drummond, M. S. (1993). Mount St. Helens: potential example of the partial melting of the subducted lithosphere in a volcanic arc. *Geology* **21**, 547–550.

Defant, M. J., Kepezhinskas, P., Defant, M. J., Xu, J. F., Kepezhinskas, P., Wang, Q., Zhang, Q. & Xiao, L. (2002). Adakites: some variations on a theme. *Acta Petrologica Sinica* **18**, 129–142.

De Sigoyer, J., Chavagnac, V., Blichert-Toft, J., Villa, I. M., Luais, B., Guillot, S., Cosca, M. & Mascle, G. (2000). Dating the Indian continental subduction and collisional thickening in the northwest Himalaya: multichronology of the Tso Morari eclogites. *Geology* **28**, 487–490.

De Wolf, C. P., Belshaw, N. S. & O'Nions, R. K. (1996). The role of inclusions in U–Pb and Sm–Nd garnet chronology: stepwise dissolution experiments and trace uranium mapping by fission track analysis. *Geochimica et Cosmochimica Acta* **60**, 121–134.

Dörr, W., Fiala, J., Vejnar, Z. & Zulauf, G. (1998). U–Pb zircon ages and structural development of metagranitoids of the Teplá crystalline complex: evidence for pervasive Cambrian plutonism within the Bohemian massif (Czech Republic). *Geologische Rundschau* **97**, 135–149.

Dörr, W., Zulauf, G., Fiala, J., Franke, W. & Vejnar, Z. (2002). Neoproterozoic to Early Cambrian history of an active plate margin in the Teplá Barrandian unit—a correlation of U–Pb

isotopic-dilution-TIMS ages (Bohemia, Czech Republic). *Tectonophysics* **352**, 65–85.

Duchêne, S., Blichert-Toft, J., Luais, B., Télouk, P., Lardeaux, J.-M. & Albarède, F. (1997). The Lu–Hf dating of garnets and the ages of the Alpine high-pressure metamorphism. *Nature* **387**, 586–589.

Eskola, P. (1920). The mineral facies of rocks. *Norsk Geologisk Tidsskrift* **6**, 143–194.

Eskola, P. (1939). Die metamorphen Gesteine. In: Barth, T. F. W., Correns, C. W. & Eskola, P. (eds) *Die Entstehung der Gesteine*. Berlin: Springer (reprint 1970), pp. 263–407.

Fernandez-Suarez, J., Corfu, F., Arenas, R., Marcos, A., Catalan, J. R. M., Garcia, F. D. & Abati, J. (2002). U–Pb evidence for a polyorogenic evolution of the HP–HT units of the NW Iberian Massif. *Contributions to Mineralogy and Petrology* **143**, 236–253.

Fiala, F. (1958). Hlavní typy hornin v širším okolí Pramenů v Císařském lese. *Geologické práce* **50**, Bratislava, 3–70.

Floyd, P. A., Winchester, J. A., Seston, R., Kryza, R. & Crowley, Q. G. (2000). Review of geochemical variation in Lower Palaeozoic metabasites from the NE Bohemian Massif: intracratonic rifting and plume–ridge interaction. In: Franke, W., Altherr, R., Haak, V. & Oncken, O. (eds) *Orogenic Processes: Quantification and Modelling in the Variscan Belt of Central Europe. Geological Society, London, Special Publications* **179**, 155–174.

Franke, W., Haak, V., Onken, O. & Tanner, D. (2000). Orogenic processes: quantification and modelling in the Variscan belt. In: Franke, W., Altherr, R., Haak, V. & Oncken, O. (eds) *Orogenic Processes: Quantification and Modelling in the Variscan Belt of Central Europe. Geological Society, London, Special Publications* **179**, 35–61.

Fraser, G., Ellis, D. & Eggins, S. (1997). Zirconium abundance in granulite-facies minerals, with implications for zircon geochronology in high-grade rocks. *Geology* **25**, 607–610.

Ganguly, J., Tirone, M. & Hervig, R. L. (1998). Diffusion kinetics of samarium and neodymium in garnet, and a method for determining cooling rates of rocks. *Science* **281**, 805–807.

Gasparik, T. & Lindsley, D. H. (1980). Phase equilibria at high pressure of pyroxenes containing monovalent and trivalent ions. In: Prewit, C. T. (ed.) *Pyroxenes. Mineralogical Society of America, Reviews in Mineralogy* **7**, 309–339.

Gebauer, D. (1990). Isotopic systems—geochronology of eclogites. In: Carswell, D. A. (ed.) *Eclogite Facies Rocks*. Glasgow: Blackie, pp. 204–224.

Gebauer, D. & Grünenfelder, M. (1979). U–Pb zircon and Rb–Sr mineral dating of eclogites and their country rocks. Example: Münchberg Gneiss Massif, Northeast Bavaria. *Earth and Planetary Science Letters* **42**, 35–44.

Gerdes, A., Wörner, G. & Henk, A. (2000). Post-collisional granite generation and HT–LP metamorphism by radiogenic heating: the example from the Variscan South Bohemian Batholith. *Journal of the Geological Society, London* **157**, 577–587.

Glodny, J., Grauert, B., Fiala, J., Vejnar, Z. & Krohe, A. (1998). Metapegmatites in the western Bohemian massif: ages of crystallisation and metamorphic overprint, as constrained by U–Pb zircon, monazite, garnet, columbite and Rb–Sr muscovite data. *Geologische Rundschau* **87**, 124–134.

Graham, C. M. & Powell, R. (1984). A garnet–hornblende geothermometer: calibration, testing, and application to the Pelona schist, Southern California. *Journal of Metamorphic Geology* **2**, 13–31.

Grauert, B., Lork, A. & O'Brien, P. (1994). Altersbestimmung akzessorischer Zirkone und Monazite aus der KTB-Vorbohrung. *KTB Report* **94-2**, B30. Hannover: Niedersächsisches Landesamt für Bodenforschung.

Green, D. H. & Ringwood, A. E. (1967). An experimental investigation of the gabbro to eclogite transformation and its petrological applications. *Geochimica et Cosmochimica Acta* **31**, 767–833.

Hawkesworth, C. J. & Vollmer, R. (1979). Crustal contamination versus enriched mantle: $^{143}Nd/^{144}Nd$ and $^{87}Sr/^{86}Sr$ evidence from the Italian Volcanics. *Contributions to Mineralogy and Petrology* **69**, 151–165.

Hawkesworth, C. J., Kempton, P. H., Rogers, N. W., Ellam, R. M. & van Calsteren, P. W. (1990). Continental mantle lithosphere, and shallow level enrichment processes in the Earth's mantle. *Earth and Planetary Science Letters* **96**, 256–268.

Heaman, L. M. & Parrish, R. R. (1991). U–Pb geochronology of accessory minerals. In: Heaman, L. M. & Ludden, J. N. (eds) *Applications of Radiogenic Isotope Systems to Problems in Geology. Mineralogical Association of Canada, Short Course Handbook* **19**, 59–102.

Hickey, R. L., Frey, F. A., Gerlach, D. C. & Lopezescobar, L. (1986). Multiple sources for basaltic arc rocks from the Southern Volcanic Zone of the Andes (34°S–41°S)—trace-element and isotopic evidence for contributions from subducted oceanic crust, mantle, and continental crust. *Journal of Geophysical Research—Solid Earth and Planets* **91**, 5963–5983.

Hofmann, A. W. (1988). Chemical differentiation of the Earth: the relation between mantle, continental crust, and ocean crust. *Earth and Planetary Science Letters* **90**, 297–324.

Holl, P. K., von Drach, V., Müller-Sohnius, D. & Köhler, H. (1989). Caledonian ages in Variscan rocks: Rb–Sr and Sm–Nd isotopic variations in dioritic intrusives from the northwestern Bohemian Massif, West Germany. *Tectonophysics* **157**, 179–194.

Humphris, S. E., Thompson, G., Schilling, J. G. & Kingsley, R. H. (1985). Petrological and geochemical variations along the Mid-Atlantic Ridge between 46°S and 32°S—influence of the Tristan da Cunha mantle plume. *Geochimica et Cosmochimica Acta* **49**, 1445–1464.

Irvine, T. N. & Baragar, W. R. A. (1971). A guide to the chemical classification of the common volcanic rocks. *Canadian Journal of Earth Sciences* **8**, 523–548.

Jelínek, E., Štědrá, V. & Cháb, J. (1997). The Mariánské Lázně Complex. In: Vrana, S. & Štědrá, V. (eds) *Geological Model of Western Bohemia Related to the KTB Borehole in Germany. Journal of Geological Sciences* **47**, 61–70.

Kachlík, V. (1997*a*). The Kladská Unit.In: Vrana, S. & Štědrá, V. (eds) *Geological Model of Western Bohemia Related to the KTB Borehole in Germany. Journal of Geological Sciences* **47**, 70–79.

Kachlík, V. (1997*b*). Contact metamorphic rocks from the mantle of the Lestkov pluton and their significance for reconstruction of the tectonometamoprhic development of the Teplá–Barrandian area (in Czech). *Geoscience Research Reports for 1996, CGS Prague*, pp. 81–82.

Kastl, E. & Tonika, J. (1984). The Mariánské Lázně metaophiolitic complex (west Bohemia). *Krystalinikum* **17**, 59–76.

Kempton, P. D., Pearce, J. A., Barry, T. L., Fitton, J. G., Langmuir, C. & Christie, D. M. (2002). Sr–Nd–Pb–Hf isotope results from ODP Leg 187: evidence for mantle dynamics of the Australian–Antarctic Discordance and origin of the Indian MORB source. *G3: Geochemistry, Geophysics, Geosystems* **3**, paper number 10.1029/2002GC000320.

Kohn, M. J. & Spear, F. S. (1990). Two new geobarometers for garnet amphibolites, with applications to southeastern Vermont. *American Mineralogist* **5**, 89–96.

Koziol, A. M. & Newton, R. C. (1988). Redetermination of the anorthite breakdown reaction and improvement of the plagioclase–garnet–Al_2SiO_5–quartz barometer. *American Mineralogist* **73**, 216–233.

Kretz, R. (1983). Symbols for rock-forming minerals. *American Mineralogist* **68**, 277–279.

Kreuzer, H., Seidel, E., Schüssler, U., Okrusch, M., Lenz, K. L. & Raschka, H. (1989). K–Ar geochronology of different tectonic units at the northwestern margin of the Bohemian Massif. *Tectonophysics* **157**, 149–178.

Kreuzer, H., Vejnar, Z., Schüssler, U., Okrusch, M. & Seidel, E. (1992). K–Ar dating on the Teplá–Domažlice Zone at the western margin of the Bohemian Massif. In: Kukal, Z. (ed.) *Proceedings of the First International Conference on the Bohemian Massif, Czech Geoogical Survey, Prague*, 168–175.

Krogh, T. E. (1982). Improved accuracy of U–Pb ages by the creation of more concordant systems using an air abrasion technique. *Geochimica et Cosmochimica Acta* **46**, 637–649.

Lapen, T. J., Mahlen, N. J., Johnson, C. M., Beard, B. L. & Baumgartner, L. P. (2002). Lu–Hf geochronology of UHP metamorphism in the Zermatt–Saas ophiolite, Lago di Cignana, Italy. *Geochimica et Cosmochimica Acta* **66**(Supplement 1), A431.

Le Roex, A. P., Dick, H. J. B., Raid, A. M., Frey, F. A., Erlank, A. J. & Hart, S. R. (1985). Petrology and geochemistry of basalts from the American–Antarctic Ridge, Southern Ocean: implications for the westward influence of the Bouvet mantle plume. *Contributions to Mineralogy and Petrology* **90**, 367–380.

Luais, B., Duchêne, S. & de Sigoyer, J. (2001). Sm–Nd disequilibrium in high-pressure, low-temperature Himalayan and Alpine rocks. *Tectonophysics* **342**, 1–22.

Ludwig, K. R. (1989). Pb.Dat: a computer program for processing raw Pb–U–Th isotope data. *US Geological Survey Open-File Report* **88**, 557.

Ludwig, K. R. (2001). User's manual for Isoplot/Ex Version 2.49, a geochronological toolkit for Microsoft Excel. *Berkeley Geochronology Center, Special Publication* **1a**.

Matte, P., Maluski, H., Reilich, P. & Franke, W. (1990). Terrane boundaries in the Bohemian Massif: results of large scale Variscan shearing. *Tectonophysics* **177**, 151–170.

Mezger, K., Hanson, G. N. & Bohlen, S. R. (1989). High precision U–Pb ages of metamorphic rutile: application to the cooling history of high-grade terranes. *Earth and Planetary Science Letters* **96**, 106–118.

Mezger, K., Essene, E. J. & Halliday, A. N. (1992). Closure temperature of the Sm–Nd system in metamorphic garnets. *Earth and Planetary Science Letters* **113**, 397–409.

Miller, J. A., Buick, I. S., Cartwright, I. & Barnicoat, A. (2002). Fluid processes during the exhumation of high-*P* metamorphic belts. *Mineralogical Magazine* **66**, 93–119.

Noble, S. R., Tucker, R. D. & Pharaoh, T. C. (1993). Lower Palaeozoic and Precambrian igneous rocks from eastern England, and their bearing on late Ordovician closure of the Tornquist Sea: constraints from U–Pb and Nd isotopes. *Geological Magazine* **130**, 835–846.

O'Brien, P. J. (1992). The formation of sapphirine and orthopyroxene during overprinting of the Mariánské Lázně Complex eclogites. *Zentralblatt für Geologie und Paläontologie* **H7/8**, 827–836.

O'Brien, P. J. (1997). Garnet zoning and reaction textures in overprinted eclogites, Bohemian Massif, European Variscides: a record of their thermal history during exhumation. *Lithos* **41**, 119–133.

O'Brien, P. J., Carswell, D. A. & Gebauer, D. (1990). Eclogite formation and distribution in the European Variscides. In: Carswell, D. A. (ed.) *Eclogite Facies Rocks*. Glasgow: Blackie, pp. 204–224.

O'Brien, P. J., Duyster, J., Grauert, B., Schreyer, W., Stöckhert, B. & Weber, K. (1997). Crustal evolution of the KTB drill site: from oldest relics to the late Hercynian granites. *Journal of Geophysical Research* **102**(B8), 18203–18220.

O'Brien, P. J. & Rötzler, J. (2003). High-pressure granulites: formation, recovery of peak conditions and implications for tectonics. *Journal of Metamorphic Geology* **21**, 3–20.

Pearce, J. A. (1983). The role of subcontinental lithosphere in magma genesis at destructive plate margins. In: Hawkesworth, C. & Norry, M. J. (eds.) *Continental Basalts and Mantle Xenoliths*. Nantwich: Shiva, pp. 230–249.

Pharaoh, T.C. (1999). Palaeozoic terranes and their lithospheric boundaries within the Trans-European Suture Zone (TESZ): a review. *Tectonophysics* **314**, 17–41.

Pidgeon, R. T. (1992). Recrystallisation of oscillatory zoned zircon: some geochronological and petrological implications. *Contributions to Mineralogy and Petrology* **110**, 463–472.

Powell, R. (1985). Regression diagnostics and robust regression in geothermometer/geobarometer calibration: the grt–cpx geothermometer revised. *Journal of Metamorphic Geology* **3**, 231–243.

Prince, C. I., Kosler, J., Vance, D. & Günther, D. (2000). Comparison of laser ablation ICP-MS and isotope dilution REE analyses—implications for Sm–Nd garnet geochronology. *Chemical Geology* **168**, 255–274.

Pupin, J. P. (1980). Zircon and granite petrology. *Contributions to Mineralogy and Petrology* **73**, 207–220.

Ringwood, A. E. (1975). *Composition and Petrology of the Earth's Mantle*. New York: McGraw–Hill.

Roberts, M. P. & Finger, F. (1997). Do U–Pb zircon ages from granulites reflect peak metamorphic conditions? *Geology* **25**, 319–322.

Roddick, J. C. (1987). Generalized numerical error analyses with applications to geochronology and thermodynamics. *Geochimica et Cosmochimica Acta* **51**, 2129–2135.

Saunders, A. D. & Tarney, J. (1979). The geochemistry of basalts from a back-arc spreading centre in the East Scotia Sea. *Geochimica et Cosmochimica Acta* **43**, 555–572.

Scherer, E. E., Mezger, K. & Münker, C. (2002). Lu–Hf ages of high pressure metamorphism in the Variscan fold belt of southern Germany. *Geochimica et Cosmochimica Acta* **66**(Supplement 1), A677.

Schmitz, M. D. & Bowring, S. A. (2000). The significance of U–Pb zircon dates in lower crustal xenoliths from the southwestern margin of the Kaapvaal craton, southern Africa. *Chemical Geology* **172**, 59–76.

Schmitz, M. D., Vervoort, J. D., Bowring, S. A. & Patchett, P. J. (2002). Decoupling of the Lu–Hf and Sm–Nd isotopic systems in granulitic lower crust beneath southern Africa. *Geochimica et Cosmochimica Acta* **66**(Supplement 1), A682.

Söllner, F. & Nelson, D. (1995). Polyphase growth history of the gneiss zircons from the continental deep drilling program (KTB): preliminary evidence from U–Th–Pb ion microprobe analyses (SHRIMP). *Terra Nova* **7**(Abstract Supplement 1), 350.

Stacey, J. S. & Kramers, J. D. (1975). Approximation of terrestrial lead isotope evolution by a two-stage model. *Earth and Planetary Science Letters* **26**, 207–221.

Štědrá, V. (2001). Tectonometamorpic evolution of the Mariánské Lázně Complex, Western Bohemia, based on the study of metabasic rocks. Ph.D. thesis, Charles University, Prague.

Štědrá, V., Kryza, R. & Kachlík, V. (2002). Coronitic metagabbros of the Mariánské Lázně Complex and Teplá Crystalline Unit: inferences for the tectonometamorphic evolution of the western margin of the Teplá–Barrandian Unit, Bohemian Massif. In: Winchester, J. A., Pharaoh, T. C. & Verniers, J. (eds) *Palaeozoic Amalgamation of Central Europe. Geological Society, London, Special Publications* **201**, 217–236.

Stosch, H.-G. & Lugmair, G. W. (1990). Geochemistry and evolution of MORB-type eclogites from the Münchberg Massif, southern Germany. *Earth and Planetary Science Letters* **99**, 230–249.

Taylor, R. N., Thirlwall, M. F., Murton, B. J., Hilton, D. R. & Gee, M. A. M. (1997). Isotopic constraints on the influence of the Icelandic plume. *Earth and Planetary Science Letters* **148**, El–E8.

Teufel, S. (1988). Vergleichende U–Pb- und Rb–Sr-Altersbestimmungen an Gesteinen des Übergangsbereiches Saxothuringikum/Moldanubikum, NE-Bayern. *Göttinger Arbeiten zur Geologie und Paläontologie* **35**, 1–87.

Teufel, S., Ahrendt, H. & Hansen, B. T. (1992). U–Pb Isotopensystematik von Monaziten aus metamorphen Gesteinen der Oberpfalz. *KTB Report* **92-4**, 319–331. Hannover: Niedersächsisches Landesamt für Bodenforschung.

Timmermann, H., Jamieson, R. A., Parrish, R. R. & Culshaw, N. G. (2002). Coeval migmatites and granulites, Muskoka domain, southwestern Grenville Province, Ontario. *Canadian Journal of Earth Sciences* **39**, 239–258.

Tonika, J. (1998). Geological map of ČR 1:50 000, sheets Mariánské Lázně and Horní Slavkov with explanations. Prague: ČGÚ.

van Breemen, O., Henderson, J. B., Loveridge, W. D. & Thompson, P. H. (1987). U–Pb zircon and monazite geochronology and zircon morphology of granulites and granite from the Thelon Tectonic Zone, Healey Lake and Artillery Lake map areas, NWT. *Current Research Part A, Geological Survey of Canada Paper* **87-1A**, 783–801.

Vavra, G. (1989). Die Entwicklung des penninischen Grundgebirges im östlichen und zentralen Tauernfenster der Ostalpen—Geochemie, Zirkonmorphologie, U/Pb Radiometrie. Dissertation, Eberhard-Karls-Universität Tübingen, 150 pp.

Vavra, G., Gebauer, D., Schmid, R. & Compston, W. (1996). Multiple zircon growth and recrystallization during polyphase Late Carboniferous to Triassic metamorphism in granulites of the Ivrea Zone (Southern Alps): an ion microprobe (SHRIMP) study. *Contributions to Mineralogy and Petrology* **122**, 337–358.

Vavra, G., Schmid, R. & Gebauer, D. (1999). Internal morphology, habit and U–Th–Pb microanalysis of amphibolite-to-granulite facies zircons: geochronology of the Ivrea Zone (Southern Alps). *Contributions to Mineralogy and Petrology* **134**, 380–404.

von Quadt, A. (1997). U–Pb zircon and Sr–Nd–Pb whole-rock investigations from the continental deep drilling (KTB). *Geologische Rundschau* **86**(Supplement), S258–S271.

Voshage, H., Hofmann, A.W., Mazzucchelli, M., Rivalenti, G., Sinigoi, S., Raczek, I. & Demarchi, G. (1990). Isotopic evidence from the Ivrea Zone for a hybrid crust formed by magmatic underplating. *Nature* **347**, 731–736.

White, W. M. (1999). Geochemistry. Lecture Notes. Cornell University (http://www.geo.cornell.edu/geology/classes/Geo656/656notes00.html).

Whitehouse, M. J. & Platt, J. P. (2003). Dating high-grade metamorphism; constraints from rare-earth elements in zircon and garnet. *Contributions to Mineralogy and Petrology*, **145**, 61–74.

York, D. (1969). Least squares fitting of a straight line with correlated errors. *Earth and Planetary Science Letters* **5**, 320–324.

Zhang, L. S. & Schärer, U. (1996). Inherited Pb components in magmatic titanite and their consequence for the interpretation of U–Pb ages. *Earth and Planetary Science Letters* **138**, 57–65.

Zulauf, G. (1997*a*). Constriction due to subduction: evidence for slab pull in the Mariánské Lázně complex (central European Variscides). *Terra Nova* **9**, 232–236.

Zulauf, G. (1997*b*). Von der Anchizone bis zur Eklogitfazies: Angekippte Krustenprofile als Folge der cadomischen und variscischen Orogenese im Teplá–Barrandium (Böhmische Masse). *Geotektonische Forschungen* **89**, 1–302.

Zulauf, G., Schitter, F., Riegler, G., Finger, F., Fiala, J. & Vejnar, Z. (1999). Age constraints on the Cadomian evolution of the Teplá Barrandian unit (Bohemian Massif) through electron microprobe dating of metamorphic monazite. *Zeitschrift der Deutschen Geologischen Gesellschaft* **150**, 627–639.

APPENDIX: ANALYTICAL METHODS

Microchemical analyses of the rock-forming minerals were made with a Camscan Link eXL energy-dispersive electron microprobe at the Czech Geological Survey. Operating conditions were 15 kV acceleration voltage, 3 nA beam current, and 40 s counting time for all elements. Natural and synthetic minerals were used for calibration and reference.

Samples (Table 1) were processed for U–Pb geochronology at the NERC Isotope Geosciences Laboratory (NIGL) in the UK using standard mineral separation techniques. All zircon fractions were abraded for up to 8 h using the air abrasion technique of Krogh (1982). Zircon, monazite, rutile, and titanite fractions were spiked with a mixed $^{205}Pb/^{233}U/^{235}U/^{230}Th$ tracer. Isotope data were obtained using the analytical procedures described by Noble *et al.* (1993) with a VG354 mass spectrometer fitted with a WARP filter and ion-counting Daly detector. Samples that yielded sufficiently large ion beams were measured in dynamic Daly–Faraday multicollector mode where ^{204}Pb was measured on the Daly detector, ^{205}Pb (and sometimes ^{207}Pb) were measured on both Daly and Faraday detectors permitting Daly/Faraday gain correction of the $^{206}Pb/^{204}Pb$ ratio, and $^{205}Pb/^{206}Pb$, $^{207}Pb/^{206}Pb$ and $^{208}Pb/^{206}Pb$ were measured on the Faraday detectors. Samples of low radiogenic Pb content yielding small ion beams were analysed in dynamic peak jumping mode on the Daly detector. Errors were calculated by numerical error propagation (Roddick, 1987), and discordia were calculated using a modified York (1969) regression. Zircon fractions Z5–Z8 of sample HT-99-6 were processed at the University of Giessen, using the analytical methods described by Dörr *et al.* (1998), including the use of a mixed $^{205}Pb/^{235}U$ spike. Analytical data are presented in Table 4. The isotope ratios are plotted using Isoplot (Ludwig, 1989, 2001); error ellipses reflect 2σ (95% confidence level) uncertainty.

Polished grain mounts for cathodoluminescence (CL) and backscatter imaging were made to detect zoning, cores, and fractures within zircon. Zircon grains were embedded in epoxy resin (Epofix) and, after hardening, were ground and polished. CL images were produced with a Zeiss DSM 962 scanning electron microscope at the GeoForschungsZentrum (GFZ) in Potsdam; backscatter images were produced with a Hitachi S500 scanning electron microscope with Link AN10,000 energy dispersive X-ray analysis system (EDS) at the University of Leicester, UK.

Sm–Nd and Sr isotope analyses were obtained in static mode on a Finnigan MAT262 multicollector mass spectrometer at the NERC Isotope Geosciences Laboratory after standard chromatographic separation. Before digestion at 120°C in a HF–HNO_3 mixture over 4 days sample powders were combined with an ^{149}Sm–^{150}Nd isotope tracer solution. Repeated analysis of an NIGL

house standard J&M, prepared from Johnson and Matthey Nd_2O_3, gave $^{143}Nd/^{144}Nd = 0{\cdot}511178 \pm 18$ (2σ, $n = 22$) during the course of this study. Samples are reported relative to a J&M value of 0·511125, which corresponds to the accepted $^{143}Nd/^{144}Nd$ of 0·511860 for the La Jolla international standard. Total analytical blanks were less than 100 pg for Nd and 400 pg for Sr. Corrections for mass fractionation were made relative to $^{146}Nd/^{144}Nd$ of 0·7219 and $^{86}Sr/^{88}Sr$ of 0·1194.

Rb and Sr trace element concentrations were obtained by X-ray fluorescence spectrometry (XRF) on pressed whole-rock powder pellets at the British Geological Survey. Major and trace element concentrations were analysed by XRF using a Philips PW 1400 system with an Rh tube at the Department of Mineralogy at Giessen University. Fused discs were used for major elements and pressed powder briquettes for Y, Zr, Nb, Ni, Cu, Zn, Ga, Pb, Th, Ba, V, and Cr.